



Tailored ASD destabilization - Balancing shelf life stability and dissolution performance with hydroxypropyl cellulose

Christian Luebbert^{a,*}, Edmont Stoyanov^b

^a amofor GmbH, Otto-Hahn-Str. 15, Dortmund D-44227, Germany

^b Nisso Chemical Europe GmbH, Berliner Allee 42, Düsseldorf D-40212, Germany

ARTICLE INFO

Keywords:

Amorphous solid dispersion
Solubility
Miscibility
PC-SAFT
Long-term stability
Hydroxypropyl cellulose
Dissolution behavior
Crystallization
Supersaturation

ABSTRACT

Amorphous solid dispersion (ASD) formulations are preferred enabling formulations for poorly water soluble active pharmaceutical ingredients (API) as they reliably enhance the dissolution behavior and solubility. Balancing a high stability against unwanted transformations such as crystallization and amorphous phase separation during storage on the one hand and optimizing the dissolution behavior of the formulation (high supersaturation and maintenance for long time) on the other hand are essential during formulation development. This study assessed the potential of ternary ASDs (one API and two polymers) containing the polymers hydroxypropyl cellulose together with poly(vinylpyrrolidone-co-vinyl acetate) (PVP VA64) or hydroxypropyl cellulose acetate succinate to stabilize the amorphously embedded APIs fenofibrate and simvastatin during storage and to enhance the dissolution performance. Thermodynamic predictions using the PC-SAFT model revealed for each combination of polymers the optimal polymer ratio, maximum API load that is thermodynamically stable as well as miscibility of the two polymers. The stability predictions were validated by three months enduring stability tests, followed by a characterization of the dissolution behavior. The thermodynamically most stable ASDs were found to be the ASDs with deteriorated dissolution performance. Within the investigated polymer combinations, physical stability and dissolution performance opposed each other.

1. Introduction

The stability against active pharmaceutical ingredient (API) crystallization during storage on the one hand and the optimal dissolution performance with fast API release on the other hand, high supersaturation and maintenance of supersaturation for a maximum period of time are key quality attributes that need to be optimized during formulation development (Vasconcelos et al., 2007; Janssens and van den Mooter, 2009).

Numerous polymer types and grades thereof are available for amorphous solid dispersion (ASD) developers. Each new API candidate requires a new ranking of the optimal polymer for the ASD formulation, either via experimental screenings of the API/polymer combinations or via in-silico tools (Page et al., 2022; Matic et al., 2020). This procedure aims at finding the optimal polymer candidate for the individual API, with optimal API load in the polymer, an optimal manufacturing process and conditions thereof, and also optimal dissolution performance. Recently marketed ASDs exhibit a broad variety of different polymers and manufacturing processes, and the optimum of both polymer and

manufacturing process must be identified individually from API to API (Vasconcelos et al., 2016; Baghel et al., 2016). Heuristic rules are usually applied to reduce the number of promising formulation candidates, but still a certain number of prototype formulations need to be assessed during this formulation development process.

Different types of release profiles may be desired, depending on the intended release profile (immediate vs. extended release) or on place of release within the gastrointestinal tract. In case of poorly-soluble API candidates, the major challenge usually is to obtain a fast initial release leading to a therapeutically effective API concentration above the low equilibrium crystalline solubility and maintaining a sufficiently high level of dissolved API (supersaturation) as long as possible by preventing recrystallization of the API (such a dissolution behavior is denoted as spring-parachute behavior) (Jadav and Paradkar, 2020; He and Ho, 2015). Both properties can be tailored by selecting appropriate polymers, e.g. for fast dissolution and/or nucleation/crystallization-inhibition purpose during storage and dissolution (Monschke and Wagner, 2020; Mansour et al., 2010).

The API stability against crystallization during storage is assessable via determining the solubility of a crystalline API in a polymer

* Corresponding author.

E-mail addresses: luebbert@amofor.de (C. Luebbert), stoyanov@nisso-chem.de (E. Stoyanov).

<https://doi.org/10.1016/j.ijpx.2023.100187>

Received 28 February 2023; Received in revised form 31 May 2023; Accepted 2 June 2023

Available online 7 June 2023

2590-1567/© 2023 The Authors. Published by Elsevier B.V. This is an open access article under the CC BY-NC-ND license (<http://creativecommons.org/licenses/by-nc-nd/4.0/>).

| Nomenclature | | Greek characters | |
|--------------------|--|------------------------------------|-----------------------------------|
| a | Helmholtz energy (J mol^{-1}) | Δ | difference (–) |
| h | molar enthalpy (J mol^{-1}) | γ | activity coefficient (–) |
| c_p | Heat capacity (J (mol K)^{-1}) | $\varepsilon^{\text{AiBi}}$ | association energy (J) |
| M | molar mass (g/mol) | ρ | density (kg m^{-3}) |
| m | segment number (–) | κ^{AiBi} | association volume (–) |
| k_B | Boltzmann constant (J K^{-1}) | σ_{seg} | segment diameter (\AA) |
| K_{GT} | Gordon-Taylor binary parameter (–) | <i>Subscripts and superscripts</i> | |
| k_{ij} | PC-SAFT binary interaction parameter (–) | assoc | associating |
| N_{assoc} | number of association sites (–) | disp | dispersion |
| R | ideal gas constant (J (mol K)^{-1}) | hc | hard chain |
| p | pressure (bar) | ij | component |
| T | temperature (K or °C) | int | intersection |
| T_g | glass-transition temperature (K or °C) | L | liquid |
| u | dispersion energy (J) | res | residual |
| w_i | mass fraction (wt%) | S | solid |
| x_i | mole fraction (mol%) | | |

(Anderson, 2018; Kyeremateng et al., 2014). ASDs with an API concentration below the solubility will never crystallize, whereas ASDs with an API concentration above the equilibrium solubility will inevitably crystallize after certain time (Prudic et al., 2014). The crystallization-onset time of a metastable ASDs determines the shelf life of the ASD and depends on the supersaturation of the API in the polymer (thermodynamic driving force to crystallize) and the molecular mobility in the ASD (kinetic risk to crystallize, depending on the glass-transition of the ASD, viscosity of the ASD and thermal history) (Wolbert et al., 2022a; Theil et al., 2017; Liu et al., 2021).

A first, fast and reliable approach to estimate the ASD stability is determining the API/polymer phase diagram with the equilibrium solubility of the API in the polymer and the glass-transition temperature of the mixture as function of composition. As the equilibrium API solubility is often lower than practically pursued API loads in formulation development, the crystallization onset time needs to be optimized by appropriate measures. One strategy to enhance the crystallization onset time is adding a second polymer to the ASD, thus generating a ternary ASD. Other strategies aim at selecting kinetically stabilizing anti-plasticizing excipients (Knapik-Kowalczyk et al., 2020) or stabilizing the glassy ASD via annealing (Flügel et al., 2020).

Adding a second polymer aims at enhancing (a) the thermodynamic stability if the API solubility in the polymer mixture is higher than in a pure polymer or (b) the glass transition of the ternary ASD compared to the one of the binary ASD (Knapik-Kowalczyk et al., 2020).

A ternary ASD might also be beneficial for the dissolution behavior of the ASD: The formulator might combine a fast releasing polymer generating a high initial API concentration in the dissolution medium with a crystallization-inhibiting polymer preventing the supersaturated API from crystallization (Janssens et al., 2008).

Formulating a ternary ASD requires additional effort during formulation development as the optimal polymer combination and the optimal ratio of the polymers need to be identified. Polymer mixtures likely tend to demix (Flory, 1953; Goh, 2014), leading to unwanted phase separation during storage. Due to high viscosities, demixing is hard to detect analytically at early stages of formulation development and requires further additional effort for quality assurance.

In this study, ternary ASDs were developed containing either HPMCAS or PVPVA64, two of the most popular polymer candidates in formulation development (approximately 40% of marketed formulations contain one of these polymers (Vasconcelos et al., 2016; Wyttenbach and Kuentz, 2017)). HPMCAS and PVPVA64 were combined with the additional polymer hydroxypropyl cellulose (HPC) grades HPC-UL (20.000 g/mol) or HPC-SSL (40.000 g/mol). HPC is a cellulosic

polymer with weak ASD physical stability stabilization potential (low API solubility in the polymer) when formulated as binary ASD (Luebbert et al., 2021), but it showed a beneficial impact on the dissolution behavior in pH-shift dissolution tests of HPMCAS/HPC/griseofulvin ternary ASDs (Zecevic et al., 2014). The two HPC grades HPC-UL and HPC-SSL are studied in this work. They are chemically identical and only differ in molar mass (HPC-UL with a molar mass of 20.000 g/mol and HPC-SSL with a molar mass of 40.000 g/mol), they are expected to behave similarly except for slight viscosity differences. HPC-containing ternary ASDs were evolving recently on the market (e.g. the sustained release ASD Isoptin® SR-E 240 from Abbott (Wyttenbach and Kuentz, 2017)).

Investigated APIs were the biopharmaceutical classification system class 2 molecules fenofibrate (FEN) and simvastatin (SIM). FEN was selected as model API known to show a poor solubility in several polymers (Theil et al., 2017; Luebbert et al., 2021). SIM was in preliminary investigations identified as API to show high solubilities in polymers. The poorly-polymer-soluble FEN is likely to crystallize during storage even at low API loads in the ASD as it shows weak interactions with polymers. SIM is highly polymer soluble and thus unlikely to crystallize even at high SIM loads in the ASD. This API selection intends to check whether strong API/polymer interactions always impair release (an API interacting strongly with polymers might be released slower as the API is stabilized in the ASD matrix (Li and Taylor, 2018)). The idea of balancing a high physical stability via strong intermolecular interactions and improving dissolution behavior via weaker intermolecular interactions was recently discussed (Deac et al., 2023; Hiew et al., 2021; Que et al., 2019; Saboo et al., 2020).

The first step of this study was a predictive in-silico screening and optimization of ternary ASDs using the thermodynamic model PC-SAFT, which was used to determine the API solubility as function of polymer composition. Additionally, the demixing behavior of the binary polymer blends and of the ASDs was predicted to ensure full miscibility in the selected ASDs.

After the storage-optimized ternary ASD compositions were identified, ternary ASDs (containing either HPMCAS or PVPVA64 and HPC) and binary reference ASDs (without HPC) were manufactured via spray drying. Each ternary mixture was manufactured at the predicted optimal polymer ratio and additionally at an 'unoptimized' polymer ratio of 50/50 (w/w). All ASDs were stored for three months at 25 °C/ 60% RH. During that time, the occurrence of crystallinity was monthly checked via differential scanning calorimetry (DSC) and powder X-ray diffraction (PXRD). Finally, the dissolution behavior of all ASDs was characterized in vitro dissolution tests.

2. Materials and methods

2.1. Materials

The APIs fenofibrate (98% purity) and simvastatin (98% purity), ethanol (96% purity) for spray drying and the buffer salts for the dissolution media were purchased from VWR International GmbH (Darmstadt). The two HPC polymers HPC-UL (20.000 g/mol) and HPC-SSL (40.000 g/mol) were provided by Nisso Chemical Europe GmbH (Düsseldorf, Germany). The polymer HPMCAS-M was obtained from ShinEtsu (SE Tylose GmbH & Co. KG, Wiesbaden, Germany), PVPVA64 was obtained from BASF SE (Ludwigshafen, Germany). Water required for dissolution experiments was filtered and deionized prior use.

2.2. Experimental characterization of binary subsystems

The phase behavior of all binary subsystems was required to confirm the PC-SAFT modeling and to determine the binary interaction parameters for the model. The solubility of the crystalline APIs in the binary subsystems FEN/HPMCAS, FEN/PVPVA64, SIM/HPMCAS, SIM/PVPVA64 and SIM/HPC was determined by heating ball-milled mixtures of each individual mixture at an API mass fraction of 60 wt% in a DSC and determining the melting offset temperature and melting enthalpy of each sample. Prior to the DSC experiments, 100 mg of powder blend were weighed with an accuracy of ± 0.1 mg into a grinding bowl and milled for 30 min at a frequency of 60 Hz in a Fritsch Pulverisette 23 (Idar-Oberstein, Germany) ball mill. This ball-milling step was performed to homogenize the API/polymer blend and reduce the particle size of the API crystals. The phase behavior of binary FEN/HPC was already characterized earlier (Luebbert et al., 2021) and is thus not investigated in detail this study. Each binary mixture was characterized at three different heating rates (1 K/min, 2 K/min, 5 K/min) with respect to offset melting temperature and this value was linearly extrapolated to 0 K/min to estimate the equilibrium solubility temperature at the known composition. All heating ramps were modulated. The heating rate modulation was set to ensure a heating-only regime (1 K/min heating rate: ± 0.159 amplitude, 2 K/min heating rate: ± 0.318 °C, 5 K/min heating rate: 0.796 °C, always 60 s modulation period). All DSC measurements were performed in open standard pans to allow solvent evaporate during the first heating ramp. The glass-transition of each mixture was obtained from the second heating ramp at 2 K/min. All DSC measurements were performed with a Q2000. DSC thermograms were evaluated with the Software TA Universal Analysis by TA Instruments (Newcastle, USA). The temperature signal was calibrated using Indium standards.

A precise determination of miscibility of two polymers is often highly challenging, and a quantitative determination of phase equilibria often impossible due to extremely slow diffusion and small domain size of evolving phases (Goh, 2014). The miscibility of the polymer blends was assessed qualitatively performing a heating/cooling/heating measurement of 50/50 (weight/weight) mixtures of each polymer blend. Immiscible blends were the blends with two glass-transitions in the second heating ramp. All samples were visually inspected for turbidity to qualitatively assess the miscibility after the DSC runs.

2.3. ASD manufacturing, storage, and dissolution

Binary reference ASDs (only containing either HPMCAS or PVPVA64 and one of the APIs FEN or SIM) and ternary ASDs (API/HPMCAS/HPC-UL, API/HPMCAS/HPC-SSL, API/PVPVA64/HPC-UL, API/PVPVA64/HPC-SSL) were manufactured via spray drying. FEN ASDs were manufactured with an API content of 15 wt%, SIM ASDs were manufactured with 40 wt% API content. All ASDs were manufactured using the spray dryer Büchi B290 (Flawil, Switzerland), which was operated at an inlet temperature of 80 °C, a feed rate of the spray-dried solution of 7 mL/min and nitrogen with a volume flow of 550 L/h fed to the atomizer nozzle.

An overview over the composition of all investigated ASDs is provided in Table S1. In total, 3 g of solid (API and the polymer(s)) were weighted with an accuracy of ± 0.1 mg in the desired ratio, dissolved in 300 ml ethanol and spray dried. Secondary drying was conducted for two days at vacuum conditions to remove any residuals.

All spray-dried ASDs were stored for twelve weeks at 25 °C. Each ASD was monthly analyzed for the occurrence of crystals via powder X-ray diffraction (PXRD) and DSC. Thus, a non-destructive technique with low level of detection (LOD) (PXRD) was combined with a destructive (due to heating) but for our investigated ASD system highly accurate analytical technique (DSC; though the DSC detection is not generally that reliable in terms of trace crystallinity detection/ nano-crystallinity detection (Moseson et al., 2021; Dedroog et al., 2020)). The DSC-measured crystallinity systematically underestimates the true crystallinity, as the miscibility of API in polymer leads to dissolution of API crystals prior to the melting event itself (this dissolution phenomenon was tried to be minimized by the fast heating ramp of 10 K/min, which is much above the heating ramp of the melting-point depression measurements). The PXRD detection limit of FEN crystals was 0.4% according to an earlier work (Luebbert et al., 2021). The measured melting enthalpy (Δh_{ASD}^{SL}) divided by the product of pure-APIs melting enthalpy (Δh_{API}^{SL}) and API mass fraction in the ASD (w_{API}) yielded the crystallinity in the ASD ($crystallinity = \Delta h_{ASD}^{SL} / (\Delta h_{API}^{SL} \cdot w_{API})$). This corresponds to the amount of API crystals per total API amount. Crystallinity in the ASDs was quantified via DSC using a linear heating ramp of 10 K/min from room temperature to 20 K above the melting temperature of the respective API. PXRD measurements were carried out with approximately 5 mg of ASD material poured on a silicon sample holder in a Rigaku MiniFlex 600 PXRD (Tokyo, Japan). Samples were scanned in a range of $5^\circ < 2\theta < 30^\circ$.

After three months of storage, the ASDs dissolution behavior was characterized in an USP2-dissolution apparatus Sotax Smart AT7 dissolution tester (Allschwil, Switzerland). A stream of dissolution medium was continuously pumped with a Sotax CY7-50 Piston Pump to UV-Vis quartz flow-through cuvettes (cuvette sample thickness 1 cm) to an Analytik Jena Specord 200 Plus UV-Vis Photometer (Jena, Germany). FEN was analyzed at a wavelength of 286 nm, SIM was analyzed at a wavelength of 237 nm. The dissolution volume was 900 mL, the dissolution test time was two hours, the paddle speed set to 75 min^{-1} , and the temperature of the dissolution medium was 37 °C. The dose of each ASD was set to a constant value of 40 mg. This corresponds to 266 mg of ASD powder in case of FEN ASDs and to 100 mg of ASD powder in case of SIM ASDs. The dissolution media were selected in accordance to the USP monographs of the respective APIs (SIM: pH 7.0 buffer solution containing 0.5% sodium dodecyl sulfate in 0.01 M sodium phosphate, FEN: pH 6.8 phosphate buffer). SIM has a reported mole fraction solubility of $1.29 \cdot 10^{-6}$ at 37 °C (approximately 30 mg/mL) (Shakeel et al., 2021), thus our SIM dissolution studies are performed almost at the equilibrium solubility (predicted amorphous solubility 270 mg/mL). FEN has an equilibrium crystalline water solubility of 0.64 mg/mL and predicted amorphous solubility of 2.72 mg/mL (both at 37 °C), it is expected to be strongly supersaturated in the dissolution medium. FEN dissolution studies are thus performed at non-sink conditions and SIM dissolution studies at sink-conditions.

2.4. Ternary ASD screening with PC-SAFT

Crystallization risk is present in an ASD as soon as the formulated API content exceeds the solubility of the crystalline API in the formulation. The crystalline solubility of an API in a polymer or multi-component mixture (e.g. in a ternary ASD) is calculated with Eq. 1 (Prausnitz et al., 1999).

$$a_{API}^{SL} = x_{API}^{SL} \gamma_{API}^{SL} = \exp \left[-\frac{\Delta h_{API}^{SL}}{R \cdot T} \left(1 - \frac{T}{T_{API}^{SL}} \right) - \frac{\Delta c_{p,API}^{SL}}{R} \left[\ln \left(\frac{T_{API}^{SL}}{T} \right) - \frac{T_{API}^{SL}}{T} + 1 \right] \right] \quad (1)$$

In this equation, x_{API}^{SL} is the mole-fraction solubility of the API in the ASD. The activity coefficient of the API γ_{API}^{SL} accounts for all intermolecular interactions between the API and all other ASD components and was obtained in this work from PC-SAFT, the product of x_{API}^{SL} and γ_{API}^{SL} is the API activity in equilibrium (a_{API}^{SL}). The melting properties of the API are the melting temperature (T_{API}^{SL}), the melting enthalpy (Δh_{API}^{SL}), and the difference of the heat capacities of the solid and liquid API ($\Delta c_{p,API}^{SL}$). R is the ideal gas constant (8.3145 J (mol K)⁻¹).

The relative driving force to crystallization (RDF) describes the thermodynamic crystallization propensity in a supersaturated ASD. A RDF of 100% is defined as the driving force in pure amorphous API and thus the highest expectable crystallization risk. The RDF decreases with decreasing API content in the ASD until reaching 0% RDF at the crystalline-solubility concentration in that ASD.

The chemical-potential difference of an API in an ASD at given API content and in the ASD with the solubility API content $\Delta\mu_{API}$ is defined by Eq. 2. This potential difference is the thermodynamic driving force to crystallize.

$$\Delta\mu_{API} = R T \ln \left(\frac{a_{API}}{a_{API}^{SL}} \right) \quad (2)$$

The relative driving force to crystallize is obtained by normalizing the driving force at a given API content by the driving force at maximum API content $\Delta\mu_{API,max}$ (100% API load) (Eq. 3).

$$RDF = \frac{\Delta\mu_{API}}{\Delta\mu_{API,max}} = \frac{\ln \left(\frac{a_{API}}{a_{SL}} \right)}{\ln \left(\frac{a_{API,max}}{a_{SL}} \right)} \quad (3)$$

The reference activity of the API $a_{API,max}$ equals one in case of a water-free ASD, as pure-component activities are always one. The equilibrium API activity a_{API}^{SL} is directly obtained from (Eq.1), a_{API} is the API activity at the given API load.

Demixing (separation into two liquid or amorphous phases L1 and L2) -especially important for ASDs that contain polymer mixtures - is calculated by Eq. 4.

$$x_i^{L1} \cdot \gamma_i^{L1} = x_i^{L2} \cdot \gamma_i^{L2} \quad (4)$$

This equation was solved simultaneously for each component i in the mixture (e.g. binary polymer blends and ternary ASDs).

The activity coefficients required for calculating thermodynamic phase equilibria and driving forces were obtained in this work using PC-SAFT. This thermodynamic model treats molecules as chains of spherical segments. Each molecule has a defined number of segments (segment number m^{seg}) with segment diameter σ and a dispersion energy parameter u/k_B describing the segment-segment interaction between molecules. PC-SAFT calculates the residual Helmholtz energy a^{res} by summing up different contributions caused by repulsion (hard chain a^{hc}), attraction (dispersion a^{disp}) and association (a^{assoc}) of the molecules (Eq. 5). The detailed expressions of the contributions can be found in literature (Gross and Sadowski, 2002; Tumakaka et al., 2002; Gross and Sadowski, 2001).

$$a^{res} = a^{hc} + a^{disp} + a^{assoc} \quad (5)$$

Contributions from interactions between unlike molecule species i and j in a mixture are calculated via the Berthelot-Lorentz mixing rules given in Eqs. 6 and 7.

$$\sigma_{ij} = \frac{1}{2} (\sigma_i + \sigma_j) \quad (6)$$

$$u_{ij} = (1 - k_{ij}) \sqrt{u_i u_j} \quad (7)$$

The dispersion energy u_{ij} is corrected via the interaction parameter k_{ij} which is fitted to experimental binary data. k_{ij} might be a constant value or linearly depends on temperature as expressed in Eq. 8.

$$k_{ij} = k_{ij,int} + k_{ij,slope} \cdot T [K] \quad (8)$$

Hydrogen bonds formed between molecules like water or APIs are considered via a defined number of donor/acceptor sites N^{assoc} . Accounting for hydrogen-bond formation between these sites requires two more model parameters, namely the association energy ϵ^{AB}/k_B and the association volume κ^{AB} . Cross association in mixtures of associating components was considered by applying mixing rules presented in Eqs.9 and 10.

$$\epsilon^{A_i B_j} = \frac{1}{2} (\epsilon^{A_i B_i} + \epsilon^{A_j B_j}) \quad (9)$$

$$\kappa^{A_i B_j} = \sqrt{\kappa^{A_i B_i} \kappa^{A_j B_j}} \left[\frac{2\sigma_{ii}\sigma_{jj}}{(\sigma_{ii} + \sigma_{jj})} \right]^3 \quad (10)$$

The glass-transition temperature (T_g) of the ASDs as function of API mass fraction w_{API} was modeled using the Gordon-Taylor Equation (Eq. 11) (Gordon and Taylor, 1952):

$$T_g = \frac{w_{API} T_{g,API} + K_{GT} w_{HPC} T_{g,HPC}}{w_{API} + K_{GT} w_{HPC}} \quad (11)$$

The Gordon-Taylor equation is only applicable for miscible mixtures, thus T_g was only modeled in those regions. The binary Gordon-Taylor parameter K_{GT} was either fitted to the obtained DSC data (in case of the PVPVA64/ HPC-UL and PVPVA64/ HPC-SSL blends) or (in case of the ASDs) predicted using the correlation $K_{GT} = \rho_{API} T_{g,API} / \rho_{HPC} T_{g,HPC}$ (ρ being the density of the amorphous substances).

3. Results and discussion

3.1. Polymer/polymer miscibility

The miscibility of the polymer mixtures PVPVA64/HPC(both grades) and HPMCAS-M/HPC was assessed experimentally and via modeling. The experimental characterization comprised a heat/cool/heat characterization of the polymer blends (50 wt% of each polymer), in which the occurrence of two separate glass transition temperatures during the second heating ramp was considered as indirect qualitative proof of immiscibility. The first heating ramp was conducted to mix and dissolve the components in each other (maximal temperature of 160 °C during first heating ramp, 40 °C above T_g of HPMCAS-M are considered as sufficient for mixing the components if miscible), the second heating ramp for evaluating the number of T_g 's. The thermograms of all polymer mixtures (HPMCAS-M/ HPC-UL, HPMCAS-M/ HPC-SSL, PVPVA64/ HPC-UL, PVPVA64/ HPC-SSL is shown in Fig. 1.

As can be seen, the second heating ramp reveals two glass-transition temperatures, one corresponding to pure HPC-UL (84.98 °C), the other corresponding to the glass-transition of pure HPMCAS-M (123.7 °C). The detection of two glass-transition temperatures in all HPC-containing blends remains challenging as the T_g step height of HPC and HPC-rich phases remains weakly detectable in DSC measurements (Luebbert et al., 2021). The PVPVA64/HPC-UL and PVPVA64/HPC-SSL base lines were almost identical across the entire temperature range, the HPMCAS-M/HPC-UL and HPMCAS-M/HPC-SSL baselines drifted away from each other at higher temperatures. One single glass-transition event is observable in PVPVA64-containing blends at approximately 109 °C, the HPMCAS-M containing blends reveal two glass-transition temperatures (one clear T_g at 122 °C, corresponding to the pure T_g of HPMCAS-M and one at lower temperature between 60 °C and 90 °C). The first and second heating ramp is shown in Fig. S3 and Fig. S4 in the Supplementary Information. Interestingly, the heat capacities differ between first and second heating ramp in case of PVPVA64/HPC-UL, this change in heat

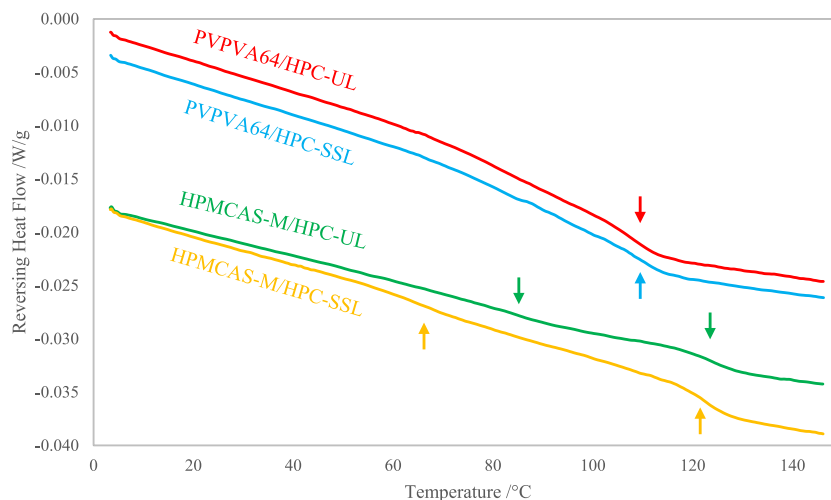


Fig. 1. DSC thermograms (reversing heat flow signals of second heating ramp) of the PVPVA64/HPC-UL (red), PVPVA64/HPC-SSL (blue), HPMCAS-M/HPC-UL (green) and HPMCAS-M/HPC-SSL (yellow) blend. The glass-transitions are marked by arrows. The thermograms were shifted on the y-axis for better visual comparability. (For interpretation of the references to colour in this figure legend, the reader is referred to the web version of this article.)

capacity may be explained by the mixing process occurring during heating (Barnum et al., 1985). A change in heat capacity is not observed in HPMCAS-M/HPC-UL blends (Fig. S4). The two glass-transition temperatures are indicator for immiscibility (at least at the high temperature of 160 °C, this does not necessarily proof miscibility at room temperature). To further assess the miscibility of the investigated blends, the samples were analyzed optically after each DSC run. The photographs of the investigated mixtures are shown in Fig. 2.

The images reveal optically clear samples in case of PVPVA64/HPC-UL and PVPVA64/HPC-SSL mixtures, thus it is concluded that those blends mixed during the heating procedure in the DSC. In contrast to these optically transparent samples, the HPMCAS-M/HPC (both grades) mixtures remained opaque. Together with the DSC analysis (Fig. 1), the 50/50 w/w mixture is concluded to be immiscible (a detailed review of optical turbidity as indicator for demixing is to be found in literature (Goh, 2014)). A further quantitative analysis of the exact compositions of the demixed polymers was not possible as the samples were constantly subjected to temperature changes in the DSC and a quantification of the concentrations in the two phases was not conducted. The predicted miscibilities/ immiscibilities of the investigated polymer blends are summarized in Table 1. The influence of API loading was not considered at this stage and the prediction serves as first screening for possible polymer compatibility.

According to Table 1, the HPMCAS-M/HPC blends (both HPC grades) are fully immiscible across the entire composition range while PVPVA64/HPC-UL blends are fully miscible across the entire composition range. The blend HPMCAS-M/PVPVA64 was predicted to be partly miscible, this means that phase separation only occurs in a certain composition range (between 70 wt% and 100 wt% PVPVA64 in the polymer blend).



Fig. 2. Photographs of the DSC pans containing the mixtures (from left to right) PVPVA64/HPC-SSL, PVPVA64/HPC-UL, HPMCAS-M/HPC-SSL and HPMCAS-M/HPC-UL taken after the DSC runs.

Table 1

Miscibility overview of the binary polymer blends at 25 °C. Miscibility was predicted with PC-SAFT using the parameters from Table 2 and Table 3.

| | PVPVA64 | HPC-SSL | HPC-UL |
|--------------------|---|------------------|----------------------------------|
| HPMCAS | Partly miscible ($0.70 < w_{PVPVA64} < 1$) | Fully immiscible | Fully immiscible |
| PVPVA64 HPC-SSL | | Fully miscible | Fully miscible Fully miscible |

The predicted phase diagrams of the two immiscible systems PVPVA64/HPMCAS-M and HPMCAS-M/HPC-UL are shown in Fig. 3.

Fig. 3 reveals the difference between a partly miscible polymer blend (PVPVA64 and HPMCAS-M, Fig. 3a) and a fully immiscible polymer blend (HPMCAS-M/HPC-UL, Fig. 3b). The miscibility gap in Fig. 3a does not cover the entire composition range and depending on the temperature, different ratios of PVPVA64 to HPMCAS-M are predicted to be fully miscible (up to 60 wt% PVPVA64 in the blend at 120 °C). A smaller miscibility gap is observed at elevated temperatures. Within the spinodal zone, spontaneous demixing occurs instantaneously. At 20 °C this highly instable region lies between $80.7 \text{ wt}\% < w_{PVPVA64} < 99.6 \text{ wt}\%$ (Fig. 3a). The equilibrium (binodal) compositions is slightly bigger, lying between $70 \text{ wt}\% < w_{PVPVA64} < 100 \text{ wt}\%$ at 20 °C.

The phase diagram of HPMCAS-M/HPC-UL (Fig. 3b) looks completely different. The spinodal and binodal branches are located at the very left and very right of the diagram. Thus, all compositions of this polymer blend are expected to demix regardless of temperature.

Based on the shape of the binary phase diagrams, a PVPVA64/HPMCAS-M blend may be considered for generating homogeneous ASD formulations in polymer composition ranges between $0 \text{ wt}\% < w_{PVPVA64}$

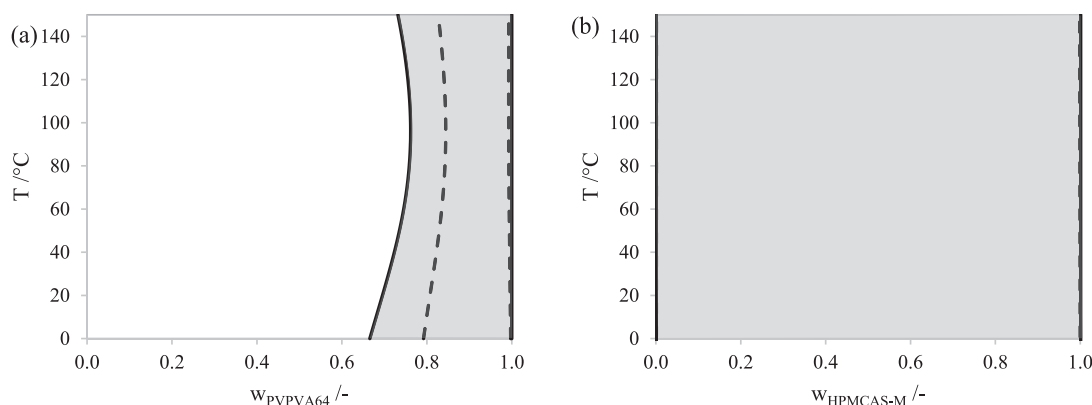


Fig. 3. PC-SAFT predicted phase diagram of PVPVA64/HPMCAS-M (a) and HPMCAS-M/HPC-UL (b). The solid black lines are the predicted binodal lines, the dashed lines are the spinodal lines. The immiscible zone is highlighted in gray.

< 70 wt% at 20 °C while the HPMCAS-M/ HPC-UL blends are always expected to phase separate regardless of the polymer ratio.

The PC-SAFT parameters used for all calculations are summarized in Table 2, the binary interaction parameters are summarized in Table 3. The melting properties of FEN required for solubility calculations were obtained from literature as given in Table 4. Gordon-Taylor interaction parameters for modeling the glass-transition temperatures of the ASDs are summarized in Table 5.

The melting properties of SIM were measured in this work via DSC. DSC thermograms of pure SIM at the three different heating rates are shown in Fig. S1. The melting enthalpy was obtained from the total heat flow signal of the measurements. The equilibrium melting temperatures were extrapolated linearly as shown in Fig. S2 to obtain the equilibrium melting temperature of pure SIM.

3.2. Solubility and glass transition of binary ASDs

The modeled solubilities of SIM in the polymers PVPVA64, HPMCAS, HPC-UL and HPC-SSL is shown in Fig. 4. The DSC thermograms leading to the presented phase diagrams are shown in the Supplementary Information (Fig. 4a: Fig. S5, Fig. 4b: Fig. S6, Fig. 4c: Fig. S7, Fig. 4d: Fig. S8).

Both the DSC measurements and the modeling revealed the strongest intermolecular interactions and thus highest SIM solubilities in PVPVA64 (Fig. 4a, 47 wt% at 25 °C), a slightly lower solubility in HPMCAS-M (Fig. 4b, 30 wt% at 25 °C), and the lowest solubility in the HPC-grades (Fig. 4c and d, solubility in both HPC-grades 22 wt% at 25 °C). All binary SIM/polymer-mixtures are miscible in the entire composition range. The solubility values at low temperatures were assessed with the method of Mohan et al (Mohan et al., 2002), evaluating the melting peak enthalpy and melting onset temperature of each DSC run. This method is expected to have higher deviations due to a high ASD viscosity/ slower dissolution at low temperatures, but enables roughly estimating solubilities at low temperatures). Below the T_g of the mixture, these values might even more deviate due to the non-

Table 2

PC-SAFT pure-component parameters of the investigated substances.

| Substance | $m_i^{seg}/M_w / \text{mol g}^{-1}$ | $\sigma_i / \text{\AA}$ | u_i/k_B /K | $\epsilon^{AiBi}/k_B / K$ | κ^{AiBi} | N_i^{assoc} (donors/ acceptors) | Parameter Ref. |
|-------------|-------------------------------------|-------------------------|-----------------|---------------------------|-----------------|-----------------------------------|--------------------------------|
| HPC-UL | 0.0447 | 2.974 | 205.00 | 1600.0 | 0.02 | 286/286 | (Luebbert et al., 2021) |
| HPC-SSL | 0.0447 | 2.974 | 205.00 | 1600.0 | 0.02 | 572/572 | (Luebbert et al., 2021) |
| fenofibrate | 0.0107 | 4.767 | 244.80 | 0 | 0.02 | 0/2 | (Brinkmann et al., 2019) |
| simvastatin | 0.0248 | 3.778 | 255.23 | 1843.1 | 0.02 | 1/1 | This work |
| HPMCAS-M | 0.0490 | 2.889 | 298.05 | 1602.3 | 0.02 | 110/110 | (Lehmkemper et al., 2017a) (*) |
| PVPVA64 | 0.0372 | 2.947 | 205.27 | 0 | 0 | 653/653 | (Lehmkemper et al., 2017b) |
| water | 0.0669 | 2.793 | 353.95 | 2425.67 | 0.0451 | 1/1 | (Cameretti and Sadowski, 2008) |

* N_i^{assoc} adapted to Shin-Etsu grade of HPMCAS-M ($M_w = 17.700 \text{ g/mol}$).

Table 3

Binary PC-SAFT interaction parameters (k_{ij}) between the investigated components.

| Component 1 | Component 2 | k_{ij} | Ref. |
|-------------|-------------|----------|----------------------------|
| Fenofibrate | water | -0.1074 | (Luebbert et al., 2021) |
| Fenofibrate | HPC-UL | 0 | (Luebbert et al., 2021) |
| Fenofibrate | PVPVA64 | 0 | |
| Fenofibrate | HPMCAS-M | -0.140 | |
| HPMCAS-M | water | -0.0358 | (Lehmkemper et al., 2017a) |
| PVPVA64 | water | -0.1560 | (Lehmkemper et al., 2017b) |
| HPC-UL | water | -0.0623 | (Luebbert et al., 2021) |
| HPC-SSL | water | -0.0623 | (Luebbert et al., 2021) |
| Simvastatin | water | -0.0789 | This work |
| Simvastatin | HPC-UL | -0.0110 | This work |
| Simvastatin | PVPVA64 | -0.0370 | This work |
| Simvastatin | HPMCAS-M | -0.0750 | This work |
| HPMCAS-M | PVPVA64 | -0.0433 | (Lehmkemper, 2018) |

Table 4

Melting properties and glass transition temperatures of the APIs fenofibrate (literature) and simvastatin (this work).

| | fenofibrate | simvastatin |
|---|--------------------------------|-------------|
| $\Delta H_{API}^{SL} / J g^{-1}$ | 92.93 (Watterson et al., 2014) | 76.85 |
| $T_{API}^{SL} / ^\circ C$ | 80.78 (Brinkmann et al., 2019) | 140.32 |
| $T_{g,API} / ^\circ C$ | -18.44 | 33.94 |
| $\Delta C_{p,API}^{SL} / J (\text{mol K})^{-1}$ | 124.3 (Watterson et al., 2014) | 230 |

equilibrium state of a glass. Also excess caloric properties are neglected by this approach.

The solubility of SIM in all polymers is significantly higher compared to the FEN solubilities (PC-SAFT calculated solubilities at 25 °C, compare Fig. 5: FEN in PVPVA64: 11 wt%, FEN in HPMCAS-M: 12 wt%, FEN in HPC: 0.8 wt% - this phase diagram was already determined in an earlier study (Luebbert et al., 2021)). Additionally, all polymers exhibit

Table 5

Gordon Taylor constants fitted in this work to the measured glass transitions of the binary mixtures.

| Mixture | K_{GT} - value |
|--------------|------------------|
| SIM/PVPVA64 | 1.10 |
| SIM/HPMCAS-M | 0.32 |
| SIM/HPC-UL | 0.12 |
| SIM/HPC-SSL | 0.12 |
| FEN/PVPVA64 | 0.32 |
| FEN/HPMCAS-M | 0.18 |

a miscibility gap with FEN, the ASDs with higher FEN loads are expected to undergo amorphous phase separation.

When comparing the two APIs SIM and FEN, the overall solubility difference in the polymers is evident and SIM reveals in general a higher solubility in the polymers.

3.3. API solubility in polymer blends

The predicted SIM solubility in polymer blends at 25 °C is shown in Fig. 6.

SIM reveals a predicted solubility maximum in the mixtures PVPVA64/HPC (both grades) and HPMCAS-M/ HPC (both grades). The solubility maximum is predicted for a polymer ratio of 90 wt% PVPVA64/ 10 wt% HPC (both grades) and 65 wt% HPMCAS-M/ 35 wt% HPC-UL. The SIM solubility in PVPVA64/HPMCAS-M reveals a weak solubility minimum at approximately 90 wt% HPMCAS-M in the PVPVA64/ HPMCAS-M mixture. The HPC mixture reveals a constant solubility regardless of HPC ratio. Thus, HPC-UL/HPC-SSL mixtures do not improve ASD stability compared to the binary HPC-containing ASDs.

The mixture PVPVA64/HMPCAS-M does not reveal improved intermolecular interactions in the mixture that stabilize such a ternary ASD against crystallization. In contrast, the polymer blends PVPVA64/HPC and HPMCAS-M/ HPC-UL reveal an enhanced stabilization potential compared to the respective pure polymers (however, the mixture HPMCAS-M/HPC demixes).

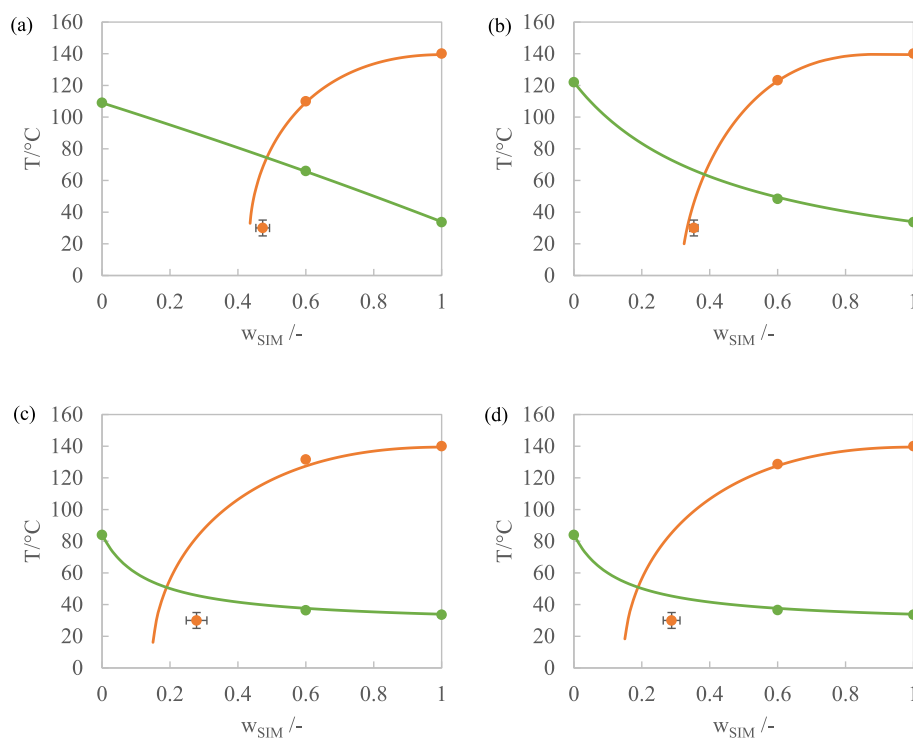


Fig. 4. Binary phase diagrams of (a) SIM/PVPVA64, (b) SIM/HPMCAS-M, (c) SIM/HPC-UL, (d) SIM/HPC-SSL. The solubility of SIM is orange, the glass-transition of the ASDs is green. Symbols are experimental values (DSC), lines are modeling (PC-SAFT: solubilities, Gordon Taylor: glass-transitions). (For interpretation of the references to colour in this figure legend, the reader is referred to the web version of this article.)

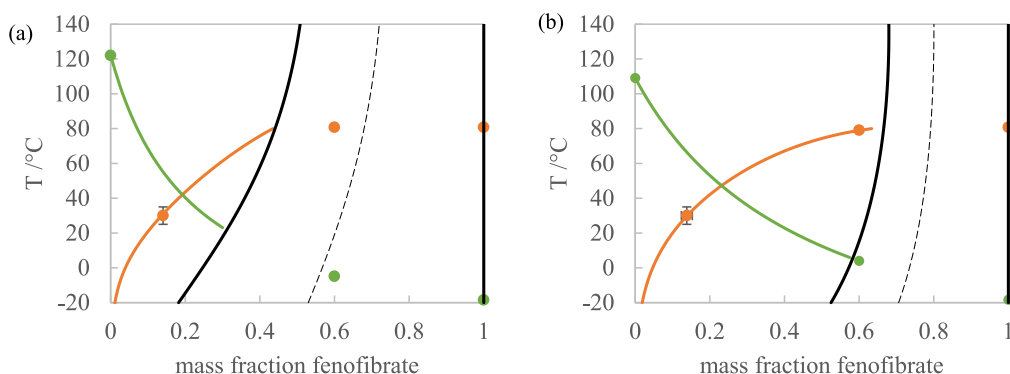


Fig. 5. Binary phase diagrams of (a) FEN/HPMCAS-M and (b) FEN/PVPVA64. The solubility of FEN is orange, the glass-transition is green, amorphous phase separation is black. Symbols are experimental values (DSC), lines are modeling (PC-SAFT solubilities, Gordon Taylor glass-transitions, amorphous phase separation occurs between the two black lines). The dashed line marks the spinodal line. (For interpretation of the references to colour in this figure legend, the reader is referred to the web version of this article.)

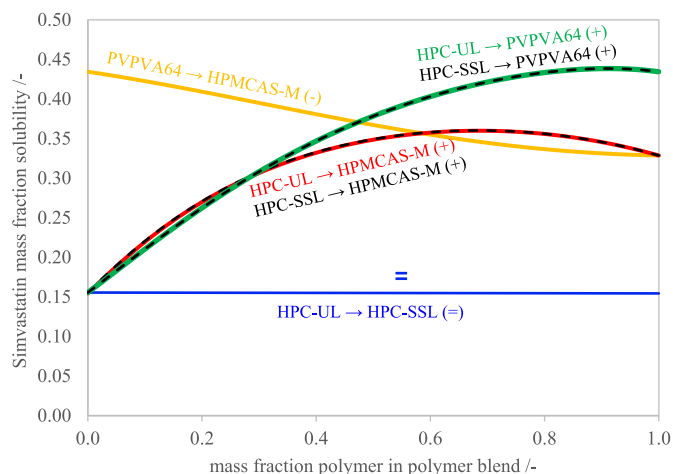


Fig. 6. Predicted SIM solubility in the investigated polymer blends as function of polymer composition at 25 °C. Beneficial solubility effects with solubility maximum are marked by (+), negative solubility effects with solubility minimum are marked by (-) and mixtures showing no influence on the solubility are marked by (=). The green line is the predicted solubility in the HPC-UL/PVPVA64 blend and the overlapping black dotted line the solubility in the HPC-SSL/PVPVA64 blend, the red line is the predicted solubility in the HPC-UL/HPMCAS-M blend and the overlapping black dotted line the solubility in the HPC-SSL/HPMCAS-M blend, the yellow line is the predicted solubility in the PVPVA64/HPMCAS-M blend and the blue line is the predicted solubility in the HPC-UL/HPC-SSL blend. (For interpretation of the references to colour in this figure legend, the reader is referred to the web version of this article.)

The screening result for the same polymer blends and FEN is shown in Fig. 7.

The HPC-mixture of the grades HPC-UL and HPC-SSL again does not influence the solubility of the API (this time FEN) and thus has no impact on the stabilization. A polymer mixtures does not show beneficial properties compared to an ASD with only one HPC grade.

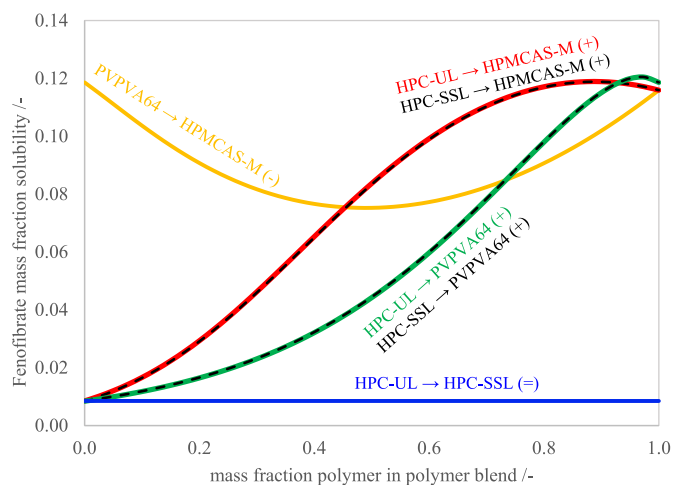


Fig. 7. Predicted FEN solubility in the investigated polymer blends as function of polymer composition at 25 °C. Mixtures with solubility maximum are marked by (+), mixtures with solubility minimum are marked by (-) and mixtures showing no influence on the solubility are marked by (=). The green line is the predicted solubility in the HPC-UL/PVPVA64 blend and the overlapping black dotted line the solubility in the HPC-SSL/PVPVA64 blend, the red line is the predicted solubility in the HPC-UL/HPMCAS-M blend and the overlapping black dotted line the solubility in the HPC-SSL/HPMCAS-M blend, the yellow line is the predicted solubility in the PVPVA64/HPMCAS-M blend and the blue line is the predicted solubility in the HPC-UL/HPC-SSL blend. (For interpretation of the references to colour in this figure legend, the reader is referred to the web version of this article.)

The PVPVA/HPMCAS-M mixture reveals a solubility minimum (besides the only partial miscibility of the polymers, compare Fig. 3b) and thus shows no beneficial properties with regard to stabilization of the amorphous state during stability testing.

The PVPVA64/HPC and HPMCAS/HPC blends reveal a solubility maximum both at low HPC concentrations (PVPVA64/HPC-UL: 5 wt% HPC, HPMCAS/HPC: 10% HPC). A beneficial stability effect is thus predicted for these specific polymer compositions. This behavior might be unexpected to the reader as HPC acts as polymeric antisolvent in the polymer blends, but such behavior is also known from solubilities in solvent/antisolvent mixtures (Dohm et al., 2021; Ruether and Sadowski, 2009). The HPC grades were not predicted to differ in their behavior, they thus reveal exactly overlapping solubility profiles.

The impact of the API interactions on the stabilization potential can be studied very well by comparing the SIM and FEN diagrams among each other. Apart from the completely different solubilities in the pure polymers (right and left hand sides of Fig. 6 and Fig. 7), also the shapes of the solubility curves in the polymer mixtures differ remarkably: PVPVA64/HPMCAS-M reveals an almost linear trend for SIM solubility, while a strong solubility minimum far below the solubilities in the individual polymers is observed for FEN (the 50/50 w/w HPMCAS-M/PVPVA64 ASD containing FEN has a solubility of 7.5 wt% compared to 1.9 wt% in PVPVA64 and 11.5 wt% in HPMCAS-M). Also, the polymer composition at which the solubility maximum is predicted differs from API to API; FEN ASDs have a solubility maximum at an HPMCAS-M content of 65 wt% in the HPMCAS-M/HPC mixture while it is 90 wt% for SIM ASDs.

3.4. Long-term stability of FEN/HPC and SIM/HPC ASDs

The long-term stability of binary reference ASDs and ternary ASDs was experimentally investigated over a period of three months. Table 6 gives an overview of the spray-dried ASDs, their predicted miscibility and crystallization behavior as well as their experimentally observed miscibility and crystallization behavior. The X-ray diffractograms after three months of storage are shown in the Supplementary Information (Fig. S9 and Fig. S10).

Table 6 reveals both the benefits and disadvantages of formulating ternary ASDs with the different investigated polymers. FEN ASDs are generally predicted to be less stable compared to SIM ASDs, although the investigated SIM load (40 wt%) was much higher than the one of the FEN ASDs (15 wt%). This is expressed by the generally higher RDF values in all FEN ASDs compared to SIM ASDs (calculated using Eq. 3).

The ternary ASDs have a stabilizing potential if a suitable polymer combination in the right polymer ratio is selected (e.g. FEN/HPMCAS-M binary reference: RDF = 23.2%; ternary FEN/HPMCAS-M/HPC-UL 50/50 w/w RDF = 43.4% (i.e. less stable), FEN/HPMCAS-M/HPC-UL 90/10 w/w RDF = 20.8% (i.e. more stable)).

The HPMCAS-M/HPC ASDs (both HPC grades) are predicted to be immiscible in the entire composition range in case of both investigated APIs. Detecting two glass-transitions is difficult due to the weak step height at HPC's pure T_g. Nevertheless, two glass-transitions were observed in SIM/HPMCAS-M/HPC-UL (35/65) and FEN/HPMCAS-M/HPC-UL (50/50). This finding validates the correctness of the PC-SAFT prediction (though the occurrence of amorphous phase separation is hard to proof in many cases analytically and miscibility claims need to be done carefully (Goh, 2014; Qian et al., 2010)). An exemplary DSC thermogram with two observed glass-transition temperatures is shown in Fig. S11 (two glass-transition temperatures and a melting peak of FEN crystals).

The SIM ASDs remained completely amorphous during the three months of storage, no signs of crystallization were observed in XRD and DSC. Only the HPMCAS-M/HPC-UL ASDs and the binary HPC-UL ASD showed trace crystallinity (max. 0.6% in the DSC), while the XRD measurements did not detect any crystallinity. A quantitative value for the SIM level of detection can thus not be provided based on the stability

Table 6
ASD long-term stability (3 months) and predicted stability parameters. The crystallinities observed after the indicated time were determined quantitatively via DSC and qualitatively via XRD (X-ray crystalline = bold numbers).

| API | Polymer 1 | Polymer 2 | API content (wt%) | Mass fraction polymer 2 in polymer mixture (wt%) | Optimized ratio: X | Predicted demixing: X | Demixing observed (2 Tg): X | API solubility in polymer mixture (wt%) | RDF (%) | Predicted max. Crystallinity (wt %) (red \geq 5%) | Crystallinity 0 months | Crystallinity 1 month | Crystallinity 2 months | Crystallinity 3 months |
|-----|-----------|-----------|-------------------|--|--------------------|-----------------------|-----------------------------|---|---------|---|------------------------|-----------------------|------------------------|------------------------|
| SIM | PVPVA64 | – | 40 | | | | | 43.4 | 0.0 | 0.0 | | | | |
| SIM | HPMCAS-M | – | 40 | | | | | 32.9 | 29.6 | 7.1 | | | | |
| SIM | HPC-UL | – | 40 | | | | | 15.5 | 69.1 | 24.5 | | 0.25% | 0.28% | 0.22% |
| SIM | PVPVA64 | HPC-UL | 40 | 50 | | | | 37.8 | 10.9 | 2.2 | | | | |
| SIM | PVPVA64 | HPC-UL | 40 | 10 | X | | | 43.8 | 0.0 | 0.0 | | | | |
| SIM | HPMCAS-M | HPC-UL | 40 | 50 | | X | | 34.9 | 19.8 | 5.1 | | 0.59% | 0.48% | 0.32% |
| SIM | HPMCAS-M | HPC-UL | 40 | 35 | X | X | X | 35.8 | 16.3 | 4.2 | | 0.11% | 0.13% | 0.14% |
| SIM | PVPVA64 | HPC-SSL | 40 | 50 | | | | 37.8 | 11.1 | 2.2 | | | | |
| SIM | PVPVA64 | HPC-SSL | 40 | 10 | X | | | 43.8 | 0.0 | 0.0 | | | | |
| SIM | HPMCAS-M | HPC-SSL | 40 | 50 | | X | | 34.9 | 20.0 | 5.1 | | | | |
| SIM | HPMCAS-M | HPC-SSL | 40 | 35 | X | X | | 35.8 | 16.5 | 4.2 | | | | |
| FEN | PVPVA64 | – | 15 | | | | | 11.9 | 15.5 | 3.1 | | 0.04% | 0.02% | 0.02% |
| FEN | HPMCAS-M | – | 15 | | | | | 11.6 | 23.2 | 3.4 | | | | |
| FEN | HPC-UL | – | 15 | | | | | 0.8 | 100.0 | 14.2 | 7.30% | 7.50% | 7.22% | 7.34% |
| FEN | PVPVA64 | HPC-UL | 15 | 50 | | | | 11.9 | 75.1 | 3.1 | | 0.04% | 0.02% | 0.02% |
| FEN | PVPVA64 | HPC-UL | 15 | 5 | X | | | 12.0 | 18.7 | 3.0 | | | | |
| FEN | HPMCAS-M | HPC-UL | 15 | 50 | | X | X | 3.0 | 43.4 | 12.0 | 2.48% | 1.53% | 1.58% | 1.75% |
| FEN | HPMCAS-M | HPC-UL | 15 | 10 | X | X | | 11.9 | 20.8 | 3.1 | | | | |
| FEN | PVPVA64 | HPC-SSL | 15 | 50 | | | | 4.4 | 75.4 | 10.6 | | 0.19% | 0.37% | 0.41% |
| FEN | PVPVA64 | HPC-SSL | 15 | 5 | X | | | 12.0 | 18.7 | 3.0 | | | | |
| FEN | HPMCAS-M | HPC-SSL | 15 | 50 | | X | X | 3.0 | 43.7 | 12.0 | 1.60% | 1.25% | 1.48% | 1.58% |
| FEN | HPMCAS-M | HPC-SSL | 15 | 10 | X | X | | 11.9 | 20.9 | 3.1 | | | | |

data (it must be at least $>0.59\%$). The FEN ASDs revealed a nice correlation between occurrence of crystallinity and RDF, high predicted RDF values correlate with higher observed crystallinities. The binary FEN/HPC-UL ASD has a RDF value of 100% (this ASD is also expected to undergo amorphous phase separation), and in line with the prediction, the observed crystallinity was high already at the beginning of the stability test. As mentioned in the methods section, the DSC determined crystallinities appear systematically underestimated: The FEN/HPC-UL ASD showed a high crystallinity of 7.3% from the beginning onwards; this value did not increase significantly and the sample was thus already close to crystallization equilibrium. The maximal predicted crystallinity in equilibrium is still twice as high (14.2%). Also the manufacturing method (spray drying) could not prevent spontaneous amorphous phase separation/crystallization. Most DSC-crystalline samples were also detected as being crystalline by XRD, only samples below 0.4% DSC crystallinity were X-ray amorphous.

The overall benefit of ternary ASDs compared to the binary ASDs is negligible in terms of physical stability, no strong stability enhancement could be achieved by addition of the second polymer. In case of FEN, where many crystalline samples were observed, the optimized polymer ratios showed a higher stability and no crystallinity compared to the 50/50 mixtures (compared to the binary PVPVA64-ASD the physical stability was equally good). The ternary ASDs with optimized polymer ratios were in most cases more stable than the 50/50 mixtures (only the SIM/HPMCAS-M/HPC-UL ASDs did not follow this trend, presumably due to simultaneously occurring amorphous phase separation). A systematic shelf-life benefit of HPC-UL over HPC-SSL could not be observed. ASDs containing one of these two grades did not differ in crystallization behavior. This observation agrees with the PC-SAFT prediction.

Fig. 8 reveals a clearly observable correlation between RDF value and crystallinity after 3 months of storage (the DSC thermograms of all SIM ASDs are shown in Fig. S12, the DSC thermograms of all FEN ASD are shown in Fig. S13). A higher RDF value correlates with higher final crystallinity. The SIM ASDs follow the trend that is observed also for FEN, measured crystallinity was highest in ASDs with highest RDF. The generally lower SIM crystallinities observed in three ASDs agree to the lower RDF values in SIM. The assessment of the RDF value thus allows fast-track estimation of the crystallization risk in an ASD. More detailed shelf-life predictions are possible when considering additional factors like the molecular mobility in the ASD (Wolbert et al., 2023; Wolbert et al., 2022b), but this precise crystallization onset time/ shelf life

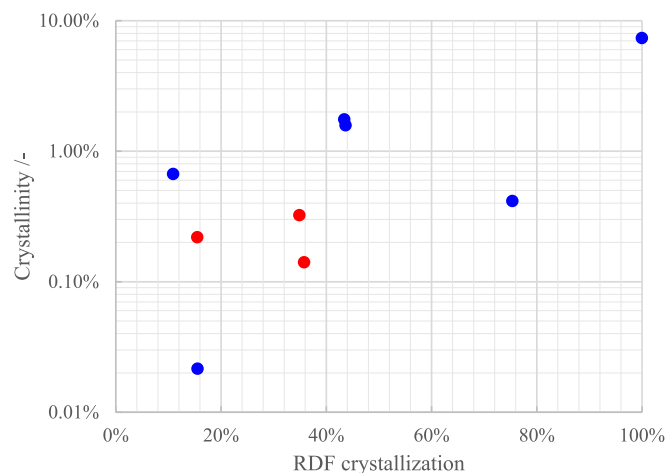


Fig. 8. DSC-determined crystallinity in the different ASDs after storage for 3 months at 25 °C as function of relative driving force to crystallization. Blue symbols are the crystallinities of the FEN ASDs and red symbols are the crystallinities of the SIM ASDs. (For interpretation of the references to colour in this figure legend, the reader is referred to the web version of this article.)

assessment was not scope of this work and thus not further investigated in detail.

3.5. Dissolution behavior

The in-vitro dissolution behavior of all ternary ASDs was investigated, their dissolution performance was compared to the dissolution behavior of the pure APIs and binary reference ASDs. The reference measurements of the pure API (40 mg API in dissolution medium) are shown in Fig. S14 in the supplementary information. The FEN concentration increased to a concentration of 0.64 mg/L during six hours, 98.4% of the weighed-in FEN powder remained undissolved during the test. The dissolution profile of crystalline SIM reveals a fast increase in SIM concentration to 44 mg/L within 20 min, this value corresponds to a complete release of the entire weighed-in SIM powder. In case of all the investigated SIM-containing ASDs, the equilibrium crystalline SIM solubility is never exceeded at any time point of the experiments in the dissolution media. Thus, all SIM molecules are expected to dissolve during the dissolution test, only the release rate may differ from ASD to ASD. The binary reference ASD release profiles (Fig. S15) show in all polymers a retarded release profile compared to pure crystalline SIM.

The FEN binary reference ASDs revealed in all cases a typical spring-parachute behavior, with fast initial release followed by a decrease in dissolved FEN concentration during the dissolution test (Fig. S16). The FEN concentration in the PVPVA64 and HPMCAS binary ASDs increased quickly after the start of the experiment and FEN dissolved completely within five minutes in both polymers. The HPC-UL ASD released at its maximum 11% FEN after 6 min. The HMCAS-M ASD revealed a decrease in FEN concentration to 10 mg/L, this value was reached after 70 min. The PVPVA64-concentration decreases at a lower rate and reaches the equilibrium value of 5.8 mg/L after 120 min. The HPC-UL ASD reveals a decrease in FEN concentration as well and reaches the equilibrium value of 3 mg/L after 20 min. The FEN/HPMCAS-M ASD was fully amorphous prior to the dissolution test, the FEN/PVPVA64 ASD was almost fully amorphous (crystallinity 0.02%), the FEN/HPC-UL ASD was crystalline (crystallinity 7.3%).

The dissolution profile of the ternary ASDs SIM/HPMCAS-M/HPC-SSL is shown in Fig. 9 together with the reference dissolution profiles of SIM/HPMCAS-M and SIM/HPC-UL.

All three binary reference ASDs (SIM/HPMCAS-M and SIM/PVPVA64 and even SIM/HPC-UL) revealed a complete dissolution within 20 to 30 min. The ternary SIM/HPMCAS-M/HPC-UL ASDs do not differ from the binary ASDs (Fig. 9a). Both ternary SIM/PVPVA64/HPC-UL ASDs (with both polymer ratios) show a strongly suppressed release after an initial dissolution of 40% SIM. The SIM concentration increases slowly to 55%–65% during one hour, but still not all API molecules dissolved completely.

Remarkably, the equally well releasing SIM/HPMCAS/HPC-UL ASDs are the ASDs with no improved physical stability (compare Table 6), while the SIM/PVPVA/HPC-UL ASD with improved physical stability dissolved even worse than the binary references: The highly stable SIM-containing ASDs do not show an improved dissolution behavior compared to the binary references. As the crystalline SIM solubility in the dissolution medium is apparently not exceeded, we postulate that the most stable (PVPVA64) ASDs show the worst dissolution behavior (release rate and final concentration), the less stable HPMCAS/HPC ASDs perform equally good as the binary references.

The investigated FEN ASD dose lead to FEN supersaturation during the dissolution experiment (the dose of 40 mg FEN exceeds the crystalline FEN solubility in pure water (0.64 mg/mL at 37 °C)), thus a supersaturation/ recrystallization profile is expected for these ASDs. The obtained dissolution curves of FEN ternary ASDs are shown in Fig. 10.

The reference HPC-UL ASD (crystallinity above 7%) shows a fast initial release up to 17%, followed by a subsequent decrease in FEN concentration until reaching the equilibrium concentration of 7% dissolved FEN after 30 min. The initially dissolved amount of FEN is very

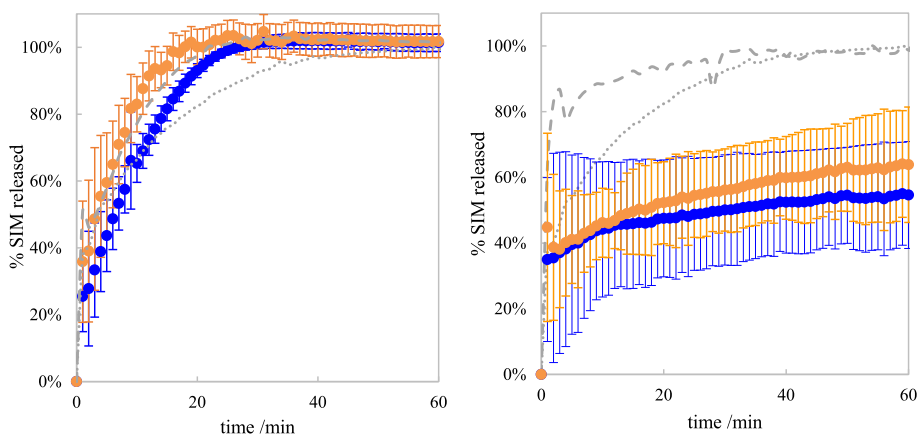


Fig. 9. Dissolution profiles of the (a) ternary SIM/HPMCAS-M/HPC-UL ASDs and (b) ternary SIM/PVPVA64/HPC-UL ASDs (100 mg ASD, 40 wt% SIM in the ASDs, dose: 40 mg SIM in 900 mL dissolution medium). Blue symbols represent the dissolution of the SIM/polymer/HPC-SSL ternary ASDs with a polymer ratio of 50/50 w/w, orange symbols represent the dissolution of the SIM/polymer/HPC-SSL ASDs with the stability-optimized polymer ratio (PVPVA64/HPC-UL:90/10; HPMAS-M:HPC-UL: 65/35, compare Table 6). The dashed line is the binary SIM/polymer reference dissolution profile, the dotted line is the binary SIM/HPC-UL-reference dissolution profile. (For interpretation of the references to colour in this figure legend, the reader is referred to the web version of this article.)

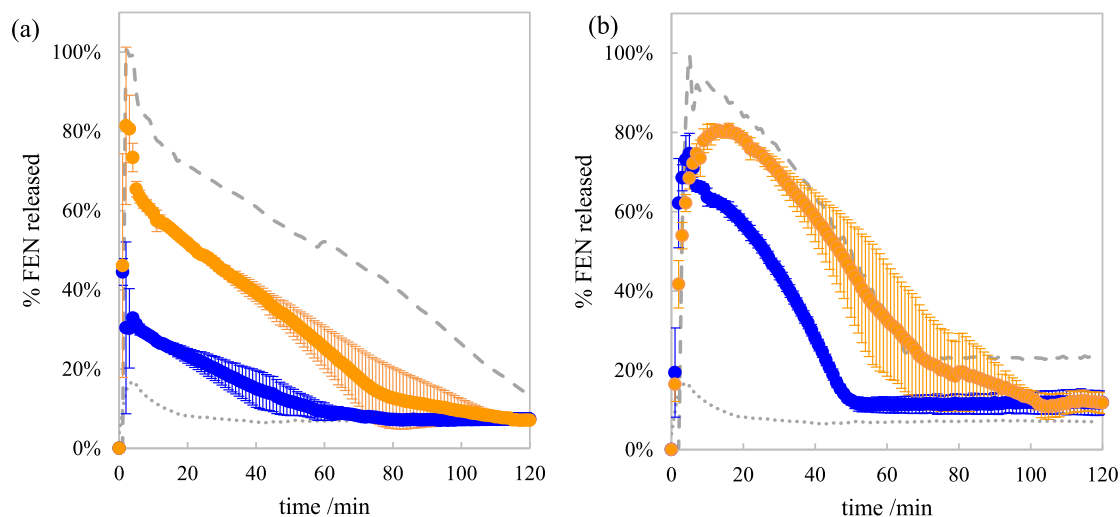


Fig. 10. Dissolution profiles of the (a) ternary FEN/PVPVA64/HPC-UL ASDs and (b) ternary FEN/HPMCAS-M/HPC-UL ASDs (266 mg ASD, 15 wt% FEN in the ASDs, dose: 40 mg FEN in 900 mL dissolution medium). Blue symbols represent the dissolution of the FEN/polymer/HPC-UL ASDs with a polymer ratio of 50/50 w/w, orange symbols represent the dissolution of the FEN/polymer/HPC-UL ASDs with the optimized ratio at 37 °C (PVPVA64/HPC-UL:95/5; HPMAS-M:HPC-UL: 90/10, compare Table 6). The dashed line is the binary FEN/polymer reference dissolution profile (a: FEN/PVPVA64, b: FEN:HPMCAS-M), the dotted line is the binary FEN/HPC-UL-reference dissolution profile. (For interpretation of the references to colour in this figure legend, the reader is referred to the web version of this article.)

low with 17% and caused by the high ASD crystallinity. The PVPVA64 and HPMCAS-M reference ASDs showed a fast initial release of almost the entire FEN amount followed by a fast recrystallization/decrease in FEN concentration (spring-parachute dissolution profile with fast and immediate initial release followed by API recrystallization). The equilibrium in the FEN/PVPVA64 ASD was not reached completely after 120 min (still 13% dissolved after 120 min, Fig. 10a, linear decrease in FEN concentration during the dissolution test), the equilibrium in the FEN/HPMCAS-M ASD was reached after 70 min (23% dissolved, Fig. 10b).

The dissolution behavior of the ternary ASDs with PVPVA64 and HPMCAS lie between its references. The area under the curves of the FEN/PVPVA64-containing dissolution profiles (Fig. 10a) follow the trend PVPVA64 > PVPVA64/HPC-UL 90/10 > PVPVA64/HPC-UL 50/50 > HPC-UL. Also, the FEN/HPMCAS-M (Fig. 10b) dissolution curves are between the binary reference profiles. The FEN/HPMCAS-M/HPC-UL ASD with 90/10 shows a retarded recrystallization between 60 and 100 min and then reaches the same equilibrium concentration as the other ternary ASD.

The finally observed equilibrium concentrations are similar in all ternary ASDs. HPC shows a retarded recrystallization behavior at the end of the tests (when much HPC is dissolved): In the binary ASDs, the concentration falls unbridled at constant rate to the equilibrium value. This concentration decrease is decelerated in the optimized ternary

ASDs. This effect is not observed at the beginning of the dissolution tests when less HPC is dissolved. Further improvements in the stabilization against recrystallization might be achieved by pre-dissolving HPC (in a tablet achievable via coating with HPC).

3.6. Comparison between HPC-UL and HPC-SSL FEN ASDs

The impact of HPC grade on the dissolution profiles of HPMCAS-M/HPC and PVPVA64/HPC grades is compared in Fig. 11.

Fig. 11 reveals in none of the polymers a significant improvement in the dissolution profiles, HPC-SSL and HPC-UL containing dissolution curves overlap within the error bars. The equilibrium is reached after longer period of time in HPMCAS-M (Fig. 11a: 100 min vs. 70 min in HPMCAS-M). The shape of the dissolution curves differs between HPMCAS and PVPVA64: HPMCAS-M reveals a fast release followed by a smooth decrease in FEN concentration, PVPVA64 reveals a steep increase followed by an almost linear decrease in concentration.

3.7. Comparison of shelf life, dissolution performance and thermodynamic properties of FEN ASDs

A brief summary and comparison between the stability and dissolution performance shall help evaluating if a ternary formulation is able

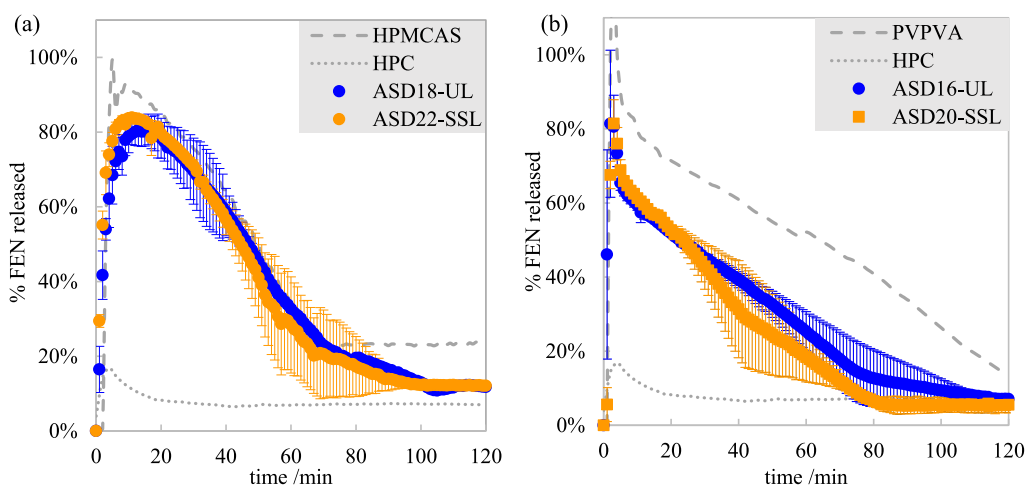


Fig. 11. Dissolution profiles of the (a) ternary FEN/HPMCAS-M/HPC ASDs and (b) ternary FEN/PVPVA64/HPC ASDs. Blue symbols represent the dissolution of the FEN/polymer/HPC-UL ASDs, orange symbols represent the dissolution of the FEN/polymer/HPC-SSL ASDs at 37 °C. The dashed line is the binary FEN/polymer reference dissolution profile, the dotted line is the binary FEN/HPC-UL reference dissolution profile. The plots were generated for the optimized polymer ratio of HPMCAS-M/HPC 90/10 w/w (a) and PVPVA64/HPC 95/5 w/w (b). (For interpretation of the references to colour in this figure legend, the reader is referred to the web version of this article.)

to enhance the ASD performance compared to binary reference ASDs. An overview over the stability and observed dissolution behavior of the ternary ASDs is provided in Table 7. The RDF value was considered to evaluate the physical stability during storage (Eq.3), the maximal FEN activity (evaluated across the hydration line) was considered to evaluate the degree of instability within the ASD during the dissolution process. The predicted API activity as function of water content is illustrated for the investigated ASDs in Fig. 12.

As can be seen in all ASDs investigated in Fig. 12, the FEN activity in all ASDs jumps abruptly during the first moments of dissolution due to the water absorption in the ASD, strongly decreasing the FEN stability in the ASD (values above 1 indicate crystallization risk). The highest degree of instability is observed for the FEN/PVPVA64 ASDs as soon as water enters the ASD, which explains the observed fast desupersaturation in the experiments (compare Fig. 11b). In contrast to this extreme ASD, the HPMCAS-M ASDs show a lower maximum FEN activity, and the HPC-ASDs reveal the lowest FEN activity among all investigated ASDs.

In the ternary PVPVA64/HPCASDs, the maximum FEN activity can be decreased remarkably (thus stabilizing FEN against crystallization), while hardly any effect of HPC could be seen in HPMCAS-M ternary ASDs.

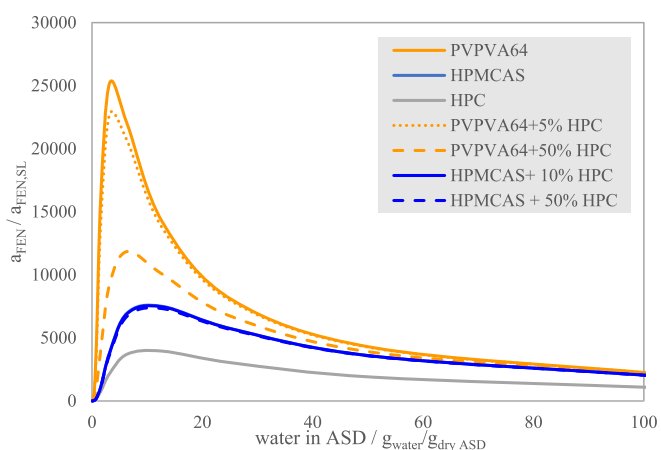


Fig. 12. Predicted API activity during the hydration process in the different investigated ASDs.

Table 7

Overview over the key characteristics (thermodynamic stability during storage and dissolution) of all ternary FEN ASDs compared to their binary reference (HPMCAS-M or PVPVA64).

| ASD | Observed Storage stability | Predicted Stability: RDF | Dissolution behavior | Max. FEN Activity During dissolution (a _{max} /a _{SL}) |
|-----------------------------|---|--------------------------|--|---|
| FEN/ PVPVA64 | Stable – fully amorphous | <0% (stable) | Immediate almost complete release; fast c _{FEN} decrease | 25,210 (high instability during initial dissolution) |
| FEN/HPC-UL | Crystallization | 100% | Low c _{max} , no high supersaturation | 3945 |
| FEN/ PVPVA64/ HPC-UL 50/50 | Trace crystallinity during storage- lower stability | 43.9% | No benefit: Dissolution curve between binary references | 11,850 |
| FEN/ PVPVA64/ HPC-UL 95/5 | Same stability (fully amorphous) | <0% (stable) | Slower recrystallization at the end, slightly better than SSL ASD | 22,735 |
| FEN/ PVPVA64/ HPC-SSL 50/50 | Trace crystallinity during storage- lower stability | 44.1% | No benefit: Dissolution curve between binary references | 11,850 |
| FEN/ PVPVA64/ HPC-SSL 95/5 | Same stability (fully amorphous) | <0% (stable) | Slower recrystallization at the end of the experiment | 22,740 |
| FEN/ HPMCAS | Stable – fully amorphous | <0% (stable) | Immediate release (c _{FEN,max} :80%) and slower c _{FEN} decrease | 7490 |
| FEN/ HPMCAS/ HPC-UL 50/50 | No benefit: Trace crystallinity during storage- lower stability | 16.9% | No benefit: Dissolution curve between binary references | 7315 |
| FEN/ HPMCAS/ HPC-UL 90/10 | Same stability (fully amorphous) | <0% (stable) | Slower recrystallization at the end of the experiment | 7455 |
| FEN/ HPMCAS/ HPC-SSL 50/50 | No benefit: Trace crystallinity during storage- lower stability | 17.2% | No benefit: Dissolution curve between binary references | 7315 |
| FEN/ HPMCAS/ HPC-SSL 90/10 | Same stability (fully amorphous) | <0% (stable) | Slower recrystallization at the end of the experiment | 7455 |

All ternary ASDs containing a 50/50 ratio of the polymers HPMCAS-M and HPC revealed lower physical stability against crystallization compared to the reference ASDs; they always contained trace crystallinity after three months of storage (the reference ASDs never revealed crystals). At the same time, the area under the curve lied in between the binary references, thus the stability was decreased while also decreasing the supersaturation during dissolution. The ternary ASDs with lower HPC content ('optimized' polymer ratio) revealed an experimentally similar (and theoretically slightly higher) stability during storage while the dissolution profiles revealed a retardation of FEN recrystallization with ongoing time of the experiments (when most of the HPC was dissolved). Crystals most likely have been present after the concentration decrease, letting conclude that HPC acts as crystal growth inhibitor in the dissolved state.

3.8. Comparison of dissolution behavior and ternary API/polymer/water phase diagrams

The shape of the API release profiles is essentially predetermined by the shape of the miscibility gap of the ternary API/polymer/water phase diagram. This phase diagram allows estimating the phenomena that occur within the ASD during dissolution as the dissolution is a coupled process of API-release from the ASD particles and simultaneous water uptake into the ASD. This water uptake might induce crucial changes within the ASD itself. To understand the dissolution behavior and polymer impact on dissolution performance also from this perspective, the predicted ternary API/polymer/water phase diagrams of the investigated binary ASDs are shown in Fig. 13.

Studying the different type ternary diagrams allows better

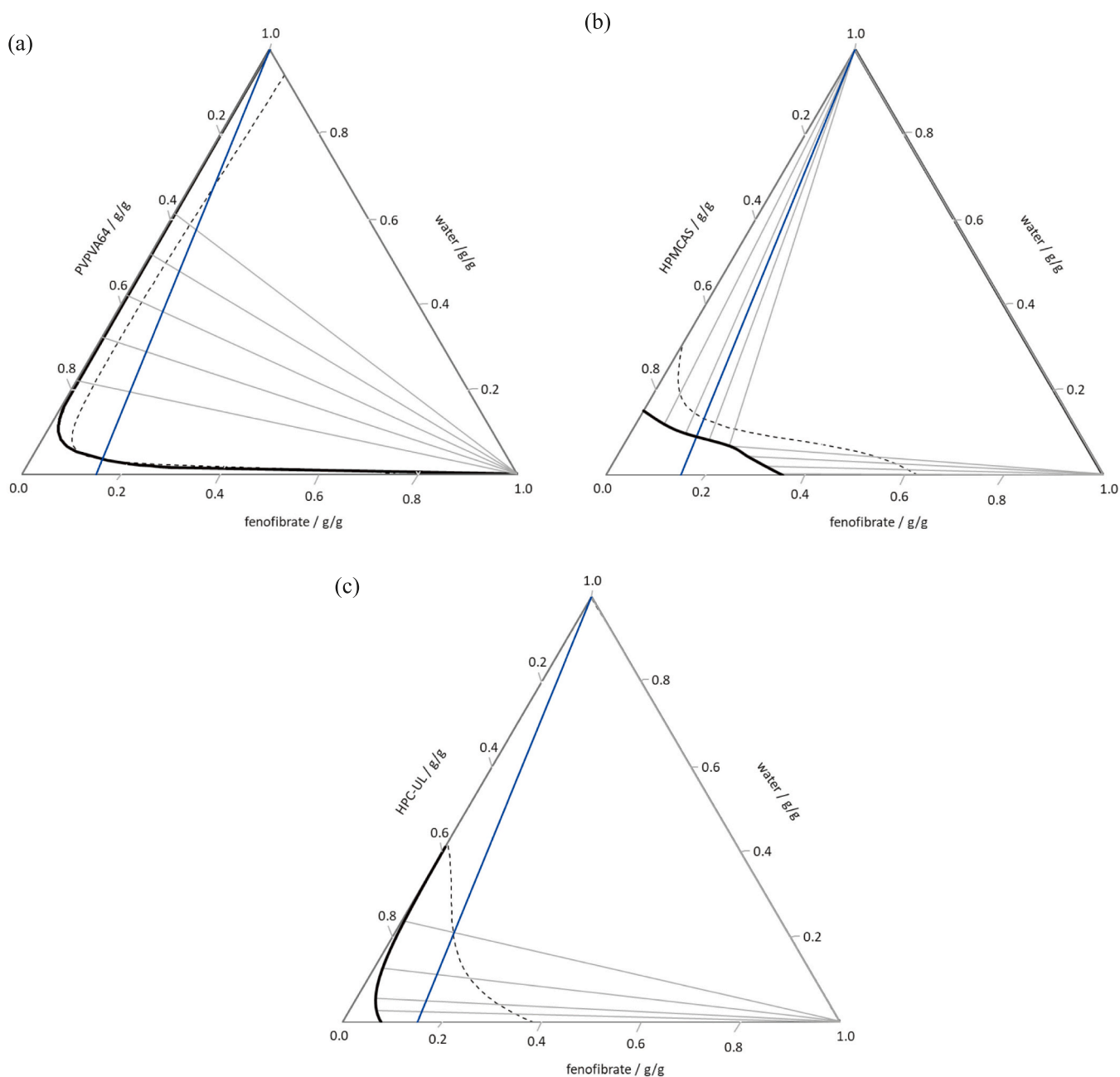


Fig. 13. PC-SAFT predicted ternary fenofibrate/polymer/water demixing behavior at 37 °C (a: PVPVA64, b: HPMCAS, c: HPC-UL). The black lines are the binodal lines, the dashed lines are the spinodal lines, the gray lines are selected tie lines, and the blue lines are the hydration lines of the ASD containing 15 wt% FEN. (For interpretation of the references to colour in this figure legend, the reader is referred to the web version of this article.)

understanding the different observed dissolution behavior of the ASDs. Depending on the polymer, the phase diagrams look completely different: The ternary diagram shown in Fig. 13a (FEN/PVPVA64/water) reveals a big miscibility gap in almost the entire composition range, the binary FEN/water mixture and also highly FEN-loaded FEN/PVPVA64 blends are immiscible (compare Fig. 5b). The investigated ASD with 15 wt% FEN load was initially fully miscible. During dissolution, water is expected to diffuse into the FEN/PVPVA64-ASD (following the hydration line) and thus the ASD enters the miscibility gap (almost in the critical point at 15 wt% FEN load in the ASD). Above this critical water content in the ASD (4 wt% water), moisture-induced phase separation is likely to occur, leading to the occurrence of a FEN-rich and PVPVA64-rich phase (in literature often observed as occurrence of turbid slurry and amorphous API nano-droplets) (Krummnow et al., 2022; Bochmann et al., 2021). With increasing water content in the ASD, the FEN load in the FEN-rich domains steadily increases and thus leads to FEN accumulation in this amorphous precipitate, while the PVPVA64-rich more hydrophilic phase completely dissolves. This explains the observed dissolution behavior of a fast initial release, followed by a fast decrease in FEN concentration due to the FEN enrichment in this hydrophobic FEN-rich phase. The FEN-rich particles are finally expected to crystallize in these precipitated particles as the FEN equilibrium solubility is exceeded (the finally expected FEN concentration is the crystalline FEN solubility in the dissolution medium containing the dissolved polymer). From a statistical viewpoint, FEN nucleation is most likely to occur in the amorphous precipitate as most FEN molecules are accumulated there.

During the dissolution test of FEN/HPMCAS-M (Fig. 13b), amorphous phase separation occurs later (more water needs to be absorbed). Interestingly, the slope of the tie line for this HPMCAS-M ASD lies now parallel to the hydration line. Thus, neither amorphous FEN can precipitate in HPMCAS-M ASDs with this FEN load nor FEN can enrich during the dissolution test. *This tie-line slope might explain the often observed high and long supersaturation levels combined with low precipitation inhibition in most HPMCAS-ASDs, making HPMCAS-M ASD dissolution behavior beneficial compared to PVPVA64-ASDs.* The HPMCAS-M/ FEN phase acts as stable amorphous reservoir which ensures a long and high FEN concentration in the dissolution medium. This beneficial behavior is only expected for a FEN load up to 35 wt,% in HPMCAS-M. Above this critical FEN load, amorphous phase separation occurs immediately, leading to spontaneous precipitation and a low supersaturation potential.

In case of HPC-UL (Fig. 13c), this precipitation (precursor to crystallization) occurs already in the water-free state as experimentally validated in the DSC and storage tests. Precipitation continues during hydration, leading to the poor observed dissolution behavior of FEN/HPC-UL ASDs. The binary mixture HPC/water is fully miscible, nevertheless, the dissolution behavior is expected to be poor with low supersaturation potential.

The ternary SIM/polymer/HPC phase diagrams were not further investigated as all SIM molecules dissolved immediately and never showed a supersaturation during the dissolution experiments.

Neither SIM ASD is thus expected to walk through a demixing zone during the dissolution process. The thermodynamic descriptor that can be assessed instead is the SIM activity in the polymer and how this evolves with increasing water content. This value reflects the intermolecular interaction strength between SIM and ASD, low values represent strong intermolecular interactions. The SIM activity in the PVPVA64-ASD has a predicted value of 0.102. The SIM activity values in HPMCAS-M and SIM in HPC-UL are predicted to be 0.24 and 0.53, respectively. With increasing water content in the particles, the SIM activity decreases in HPMCAS-M and HPC-UL (and SIM is thus stronger stabilized in the matrix instead of being released into the aqueous phase) and increases in case of PVPVA64 (making it favorable to dissolve SIM in the aqueous phase). This behavior is contrary to the FEN-ASDs, where the FEN activity immediately increased in the matrix during hydration

(compare Fig. 12).

The release behavior of the FEN and SIM ASDs cannot be quantitatively explained or even predicted by thermodynamic descriptors only. Thermodynamic activities and ternary phase diagrams are still considered as reasonable tool to explain intermolecular-interaction based phenomena associated with the dissolution process.

4. Conclusions

The stability and dissolution behavior of ternary ASDs containing the APIs Simvastatin and Fenofibrate, one of the polymers PVPVA64 or HPMCAS and the polymers HPC-UL or HPC-SSL was investigated in this work. Thermodynamic modeling was conducted to assess the stability (crystallization risk and miscibility) and potential stabilization potential of the ternary ASDs and to identify the best-stabilizing polymer ratio for each ASD. While the binary PVPVA64 and HPMCAS-ASDs remained amorphous during storage and thus revealed a high storage stability, the binary HPC-ASDs (both HPC grades) were less stable and crystallized quickly. Ternary ASDs containing the polymers PVPVA64/HPC and HPMCAS-M/HPC revealed in the prediction a slight solubility maximum. The solubility maximum and thus optimal composition depended on the investigated API and low HPC-concentrations show the highest solubility maxima. High HPC-concentrations act as anti-solubilizing polymer, enhancing the crystallization risk in the ASDs (also observed during stability tests). On the one hand, an addition of HPC acted as destabilizing agent with respect to storage stability, on the other hand we observed an API recrystallization preventing effect of dissolved HPC during the dissolution experiments (strongest at the end of the experiments). In case of Simvastatin ASDs, we observed strong depression of the dissolution performance (slower release and lower final concentration), which is unfavorable from the dissolution point of view, while the long-term stability of ASDs could be enhanced even for a higher SIM load compared to FEN ASDs (high SIM solubility in many polymers). Successful ASD formulations must ensure a sufficient storage stability and good dissolution performance (fast release and slow recrystallization velocity) at the same time. This goal is often diametral and difficult to achieve with only one polymeric excipient, as a strong storage stabilizer (e.g. PVPVA64, HPMCAS-M) or well stabilizable API (FEN) can often act as dissolution-impairing agent (the strong intermolecular interactions in the ASD make a release more difficult). HPC acts as storage stability destabilizing excipient in ASDs (promoting crystallization/phase separation), but can stabilize the recrystallization behavior of the API during dissolution (as it weakly interacts with the API molecules in the dissolved state). Both HPC polymer grades with molar masses of 20.000 g/mol (HPC-UL) and 40.000 g/mol (HPC-SSL) behaved similar in our study. When tailoring both the stability and dissolution performance, HPC can be incorporated to balance a sufficient stability during storage with a better dissolution performance. HPC is not the perfect stability/dissolution mediator according to this study, and combinations like PVPVA64/HPMCAS-M or PVP/HPMCAS (Xie and Taylor, 2016) might be evaluated as alternatives in future studies. A tailored ASD destabilization seems counter-intuitive, but might lead to a better balance between sufficient shelf-life and still a good dissolution performance in future formulations.

CRedit authorship contribution statement

Christian Luebbert: Conceptualization, Methodology, Software, Validation, Formal analysis, Investigation, Data curation, Writing – original draft, Visualization, Project administration. **Edmont Stoyanov:** Conceptualization, Methodology, Validation, Resources, Writing – review & editing, Funding acquisition.

Declaration of Competing Interest

The authors declare the following financial interests/personal

relationships which may be considered as potential competing interests.

Christian Luebbert reports financial support was provided by Nisso Chemical Europe GmbH. Christian Luebbert reports a relationship with Nisso Chemical Europe GmbH that includes: funding grants.

Data availability

Data will be made available on request.

Acknowledgement

This work was funded by Nisso Chemical Europe GmbH, Düsseldorf, Germany. amofor GmbH and Nisso Chemical Europe GmbH participated in study design, research, interpretation of data, writing, data collection, analysis, reviewing, and approving the publication. PC-SAFT calculations were performed using the software Solcalc (amofor GmbH, Dortmund, Germany). The authors thank Prof. Gabriele Sadowski for constructive discussions and the feedback on this work.

Appendix A. Supplementary data

Supplementary data to this article can be found online at <https://doi.org/10.1016/j.ijpx.2023.100187>.

References

- Anderson, B.D., 2018. Predicting Solubility/Miscibility in Amorphous Dispersions: it is Time to move beyond regular solution Theories. *J. Pharm. Sci.* 107 (1), 24–33. <https://doi.org/10.1016/j.xphs.2017.09.030>.
- Baghel, S., Cathcart, H., O'Reilly, N.J., 2016. Polymeric amorphous solid dispersions: a review of amorphization, crystallization, stabilization, solid-state characterization, and aqueous solubilization of biopharmaceutical classification system class II Drugs. *J. Pharm. Sci.* 105 (9), 2527–2544. <https://doi.org/10.1016/j.xphs.2015.10.008>.
- Barnum, R.S., Goh, S.H., Barlow, J.W., Paul, D.R., 1985. Excess heat capacities for two miscible polymer blend systems. *J. Polym. Sci. B Polym. Lett. Ed.* 23 (8), 395–401. <https://doi.org/10.1002/pol.1985.130230801>.
- Bochmann, E.S., Steidel, A., Rosenblatt, K.M., Gessner, D., Liepold, B., 2021. Assessment of the amorphous solid dispersion erosion behavior following a novel small-scale predictive approach. *Eur. J. Pharm. Biopharm.* 158, 105682. <https://doi.org/10.1016/j.ejps.2020.105682>. Published Online: Dec. 23, 2020.
- Brinkmann, J., Huxoll, F., Luebbert, C., Sadowski, G., 2019. Solubility of pharmaceutical ingredients in triglycerides. *Eur. J. Pharm. Biopharm.* 145, 113–120. <https://doi.org/10.1016/j.ejpb.2019.10.012>.
- Cameretti, L.F., Sadowski, G., 2008. Modeling of aqueous amino acid and polypeptide solutions with PC-SAFT. *Chem. Eng. Process. Process Intensif.* 47 (6), 1018–1025. <https://doi.org/10.1016/j.ccep.2007.02.034>.
- Deac, A., Qi, Q., Indulkar, A.S., Purohit, H.S., Gao, Y., Zhang, G.G.Z., Taylor, L.S., 2023. Dissolution mechanisms of amorphous solid dispersions: role of drug load and molecular interactions. *Mol. Pharm.* 20 (1), 722–737. <https://doi.org/10.1021/acs.molpharmaceut.2c00892>. Published Online: Dec. 22, 2022.
- Deedro, S., Pas, T., Vergauwen, B., Huygens, C., van den Mooter, G., 2020. Solid-state analysis of amorphous solid dispersions: Why DSC and XRPD may not be regarded as stand-alone techniques. *J. Pharm. Biomed. Anal.* 178, 112937. <https://doi.org/10.1016/j.jpba.2019.112937>. Published Online: Oct. 18, 2019.
- Dohrn, S., Luebbert, C., Lehmkemper, K., Kyeremateng, S.O., Degenhardt, M., Sadowski, G., 2021. Solvent mixtures in pharmaceutical development: Maximizing the API solubility and avoiding phase separation. *Fluid Phase Equilib.* 548, 113200. <https://doi.org/10.1016/j.fluid.2021.113200>.
- Flory, P.J., 1953. *Principles of Polymer Chemistry*, 1. Publ. 1953, 20. print. Cornell Univ. Press.
- Flügel, K., Hennig, R., Thommes, M., 2020. Impact of structural relaxation on mechanical properties of amorphous polymers. *Eur. J. Pharm. Biopharm.* 2020 (154), 214–221. <https://doi.org/10.1016/j.ejpb.2020.07.016>. Published Online: Jul. 20.
- Goh, S.H., 2014. Miscible polymer blends. In: Utracki, L.A., Wilkie, C.A. (Eds.), *Polymer Blends Handbook*. Springer Netherlands, pp. 1915–2151. https://doi.org/10.1007/978-94-007-6064-6_24.
- Gordon, M., Taylor, J.S., 1952. Ideal copolymers and the second-order transitions of synthetic rubbers. I. non-crystalline copolymers. *J. Appl. Chem.* 2, 493–500. <https://doi.org/10.1002/jctb.5010020901>.
- Gross, J., Sadowski, G., 2001. Perturbed-chain SAFT: an equation of state based on a perturbation theory for chain molecules. *Ind. Eng. Chem. Res.* 40, 1244–1260. <https://doi.org/10.1021/ie0003887>.
- Gross, J., Sadowski, G., 2002. Application of the Perturbed-Chain SAFT Equation of State to Associating Systems. *Ind. Eng. Chem. Res.* 41 (22), 5510–5515. <https://doi.org/10.1021/ie010954d>.
- He, Y., Ho, C., 2015. Amorphous Solid Dispersions: utilization and challenges in Drug Discovery and Development. *J. Pharm. Sci.* 104 (10), 3237–3258. <https://doi.org/10.1002/jps.24541>.
- Hiew, T.N., Zemlyanov, D.Y., Taylor, L.S., 2021. Balancing solid-state stability and dissolution performance of lumefantrine amorphous solid dispersions: the role of polymer choice and drug-polymer interactions. *Mol. Pharm.* <https://doi.org/10.1021/acs.molpharmaceut.1c00481>. Published Online: Sep. 8, 2021.
- Jadav, N.B., Paradkar, A., 2020. Solid dispersions: technologies used and future outlook. In: *Nanopharmaceutics*. Elsevier, pp. 91–120. <https://doi.org/10.1016/B978-0-12-817778-5.00005-1>.
- Janssens, S., van den Mooter, G., 2009. Review: physical chemistry of solid dispersions. *J. Pharm. Pharmacol.* 61 (12), 1571–1586. <https://doi.org/10.1211/jpp/61.12.0001>.
- Janssens, S., Armas, H.N., de D'Autry, W., van Schepdael, A., van den Mooter, G., 2008. Characterization of ternary solid dispersions of Itraconazole in polyethylene glycol 6000/polyvidone-vinylacetate 64 blends. *Eur. J. Pharm. Biopharm.* 69, 1114–1120. <https://doi.org/10.1016/j.ejpb.2008.02.007>.
- Knapik-Kowalczyk, J., Chmiel, K., Pacult, J., Bialek, K., Tajber, L., Paluch, M., 2020. Enhancement of the Physical Stability of Amorphous Sildenafil in a Binary Mixture, with either a Plasticizing or Antiplasticizing compound. *Pharmaceutics* 12 (5). <https://doi.org/10.3390/pharmaceutics12050460>.
- Krummow, A., Danzer, A., Voges, K., Dohrn, S., Kyeremateng, S.O., Degenhardt, M., Sadowski, G., 2022. Explaining the release mechanism of Ritonavir/PVPVA amorphous solid dispersions. *Pharmaceutics* 14 (9). <https://doi.org/10.3390/pharmaceutics14091904>. Published Online: Sep. 8, 2022.
- Kyeremateng, S.O., Pudlas, M., Woehrl, G.H., 2014. A fast and reliable empirical approach for estimating solubility of crystalline drugs in polymers for hot melt extrusion formulations. *J. Pharm. Sci.* 103, 2847–2858. <https://doi.org/10.1002/jps.23941>.
- Lehmkemper, K., 2018. *Physical stability of amorphous solid dispersions*. In: *Auflage: Schriftenreihe Thermodynamik, Band 21; Verlag Dr. Hut*, 1.
- Lehmkemper, K., Kyeremateng, S.O., Heinzlering, O., Degenhardt, M., Sadowski, G., 2017a. Impact of polymer type and relative humidity on the long-term physical stability of amorphous solid dispersions. *Mol. Pharm.* 14 (12), 4374–4386. <https://doi.org/10.1021/acs.molpharmaceut.7b00492>. Published Online: Nov. 7, 2017.
- Lehmkemper, K., Kyeremateng, S.O., Heinzlering, O., Degenhardt, M., Sadowski, G., 2017b. Long-term physical stability of PVP- and PVPVA-amorphous solid dispersions. *Mol. Pharm.* 14 (1), 157–171. <https://doi.org/10.1021/acs.molpharmaceut.6b00763>. Published Online: Dec. 7, 2016.
- Li, N., Taylor, L.S., 2018. Tailoring supersaturation from amorphous solid dispersions. *J. Control. Release* 2018 (279), 114–125. <https://doi.org/10.1016/j.jconrel.2018.04.014>. Published Online: Apr. 11.
- Liu, B., Theil, F., Lehmkemper, K., Gessner, D., Li, Y., van Lishaut, H., 2021. Crystallization risk assessment of amorphous solid dispersions by physical shelf-life modeling: a practical approach. *Mol. Pharm.* 18 (6), 2428–2437. <https://doi.org/10.1021/acs.molpharmaceut.1c00270>. Published Online: May. 25, 2021.
- Luebbert, C., Stoyanov, E., Sadowski, G., 2021. Phase behavior of ASDs based on hydroxypropyl cellulose. *Int. J. Pharm. X* (3), 100070. <https://doi.org/10.1016/j.ijpx.2020.100070>. Published Online: Dec. 19, 2020.
- Mansour, H.M., Sohn, M., Al-Ghananeem, A., DeLuca, P.P., 2010. Materials for pharmaceutical dosage forms: molecular pharmaceutics and controlled release drug delivery aspects. *Int. J. Mol. Sci.* 11 (9), 3298–3322. <https://doi.org/10.3390/ijms11093298>. Published Online: Sep. 15, 2010.
- Matić, J., Paudel, A., Bauer, H., García, R.A.L., Biedrzycka, K., Khinast, J.G., 2020. Developing HME-Based Drug Products using Emerging Science: a Fast-Track Roadmap from Concept to Clinical batch. *AAPS PharmSciTech* 21 (5), 176. <https://doi.org/10.1208/s12249-020-01713-0>.
- Mohan, R., Lorenz, H., Myerson, A.S., 2002. Solubility Measurement using Differential Scanning Calorimetry. *Ind. Eng. Chem. Res.* 41 (19), 4854–4862. <https://doi.org/10.1021/ie0200353>.
- Monschke, M., Wagner, K.G., 2020. Impact of HPMCAS on the Dissolution Performance of polyvinyl Alcohol Celecoxib Amorphous Solid Dispersions. *Pharmaceutics* 12 (6). <https://doi.org/10.3390/pharmaceutics12060541>.
- Moseson, D.E., Corum, I.D., Lust, A., Altman, K.J., Hiew, T.N., Eren, A., Nagy, Z.K., Taylor, L.S., 2021. Amorphous solid dispersions containing residual crystallinity: competition between dissolution and matrix crystallization. *AAPS J.* 23 (4), 69. <https://doi.org/10.1208/s12248-021-00598-6>. Published Online: May. 17, 2021.
- Ditzinger, F., 2022. Structured development approach for amorphous systems. In: Page, S., Maurer, R., Wyttenbach, N., Williams III, R.O., Davis, D.A., Miller, D.A. (Eds.), *Formulating Poorly Water Soluble Drugs*. AAPS Advances in the Pharmaceutical Sciences Series; Springer International Publishing, pp. 287–326. https://doi.org/10.1007/978-3-030-88719-3_8.
- Prausnitz, J.M., Lichtenthaler, R.N., Azevedo, E.G., d., 1999. *Molecular thermodynamics of fluid-phase equilibria*. In: *Prentice-Hall International Series in the Physical and Chemical Engineering Sciences*, 3rd ed. Prentice Hall PTR.
- Prudic, A., Ji, Y., Sadowski, G., 2014. Thermodynamic phase Behavior of API/Polymer Solid Dispersions. *Mol. Pharm.* 11, 2294–2304. <https://doi.org/10.1021/mp400729x>.
- Qian, F., Huang, J., Zhu, Q., Haddadin, R., Gawel, J., Garmise, R., Hussain, M., 2010. Is a distinctive single Tg a reliable indicator for the homogeneity of amorphous solid dispersion? *Int. J. Pharm.* 395, 232–235. <https://doi.org/10.1016/j.ijpharm.2010.05.033>.
- Que, C., Lou, X., Zemlyanov, D.Y., Mo, H., Indulkar, A.S., Gao, Y., Zhang, G.G.Z., Taylor, L.S., 2019. Insights into the dissolution behavior of ledipasvir-copovidone amorphous solid dispersions: role of drug loading and intermolecular interactions. *Mol. Pharm.* 16 (12), 5054–5067. <https://doi.org/10.1021/acs.molpharmaceut.9b01025>. Published Online: Nov. 18, 2019.

- Ruether, F., Sadowski, G., 2009. Modeling the solubility of pharmaceuticals in pure solvents and solvent mixtures for drug process design. *J. Pharm. Sci.* 98 (11), 4205–4215. <https://doi.org/10.1002/jps.21725>.
- Saboo, S., Kestur, U.S., Flaherty, D.P., Taylor, L.S., 2020. Congruent release of drug and polymer from amorphous solid dispersions: insights into the role of drug-polymer hydrogen bonding, surface crystallization, and glass transition. *Mol. Pharm.* 17 (4), 1261–1275. <https://doi.org/10.1021/acs.molpharmaceut.9b01272>. Published Online: Mar. 17, 2020.
- Shakeel, F., Alshehri, S., Ibrahim, M.A., Altamimi, M., Haq, N., Elzayat, E.M., Shazly, G. A., 2021. Solubilization and thermodynamic properties of simvastatin in various micellar solutions of different non-ionic surfactants: Computational modeling and solubilization capacity. *PLoS One* 16 (4), e0249485. <https://doi.org/10.1371/journal.pone.0249485>. Published Online: Apr. 8, 2021.
- Theil, F., Milsmann, J., Kyeremateng, S.O., Anantharaman, S., Rosenberg, J., van Lishaut, H., 2017. Extraordinary Long-Term-Stability in Kinetically Stabilized Amorphous Solid Dispersions of Fenofibrate. *Mol. Pharm.* 14 (12), 4636–4647. <https://doi.org/10.1021/acs.molpharmaceut.7b00735>.
- Tumakaka, F., Gross, J., Sadowski, G., 2002. Modeling of polymer phase equilibria using Perturbed-Chain SAFT. *Fluid Phase Equilib.* 194–197, 541–551. [https://doi.org/10.1016/S0378-3812\(01\)00785-3](https://doi.org/10.1016/S0378-3812(01)00785-3).
- Vasconcelos, T., Sarmento, B., Costa, P., 2007. Solid dispersions as strategy to improve oral bioavailability of poor water soluble drugs. *Drug Discov. Today* 12, 1068–1075. <https://doi.org/10.1016/j.drudis.2007.09.005>.
- Vasconcelos, T., Marques, S., das Neves, J., Sarmento, B., 2016. Amorphous solid dispersions: Rational selection of a manufacturing process. *Adv. Drug Deliv. Rev.* 100, 85–101. <https://doi.org/10.1016/j.addr.2016.01.012>.
- Watterson, S., Hudson, S., Svård, M., Rasmuson, Å.C., 2014. Thermodynamics of fenofibrate and solubility in pure organic solvents. *Fluid Phase Equilib.* 367, 143–150. <https://doi.org/10.1016/j.fluid.2014.01.029>.
- Wolbert, F., Fahrig, I.-K., Gottschalk, T., Luebbert, C., Thommes, M., Sadowski, G., 2022a. Factors Influencing the Crystallization-Onset Time of Metastable ASDs. *Pharmaceutics* 14 (2), 269. <https://doi.org/10.3390/pharmaceutics14020269>.
- Wolbert, F., Nikoleit, K., Steinbrink, M., Luebbert, C., Sadowski, G., 2022b. The shelf life of ASDs: 1. Measuring the crystallization kinetics at humid conditions. *Mol. Pharm.* 19 (7), 2483–2494. <https://doi.org/10.1021/acs.molpharmaceut.2c00188>. Published Online: Jun. 21, 2022.
- Wolbert, F., Luebbert, C., Sadowski, G., 2023. The Shelf Life of ASDs: 2. Predicting the shelf life at storage conditions.
- Wytenbach, N., Kuentz, M., 2017. Glass-forming ability of compounds in marketed amorphous drug products. *Eur. J. Pharm. Biopharm.* 112, 204–208. <https://doi.org/10.1016/j.ejpb.2016.11.031>.
- Xie, T., Taylor, L.S., 2016. Dissolution performance of high drug loading celecoxib amorphous solid dispersions formulated with polymer combinations. *Pharm. Res.* 33 (3), 739–750. <https://doi.org/10.1007/s11095-015-1823-y>. Published Online: Nov. 12, 2015.
- Zecevic, D.E., Meier, R., Daniels, R., Wagner, K.-G., 2014. Site specific solubility improvement using solid dispersions of HPMC-AS/HPC SSL-mixtures. *Eur. J. Pharm. Biopharm.* 87 (2), 264–270. <https://doi.org/10.1016/j.ejpb.2014.03.018>. Published Online: Apr. 21, 2014.